AD-A150 565 INTERLAMINAR FRACTURE TOGGHNESS IN RESIN MATRIX COMPOSITES(U) GEORGIA INST OF TECH ATLANTA SCHOOL OF AEROSPACE ENGINEERING L W REHFIELD ET AL. APR 84 1/1

UNCLASSIFIED AFOSR-TR-85-0061 AFOSR-83-0056 F/G 11/4 NL

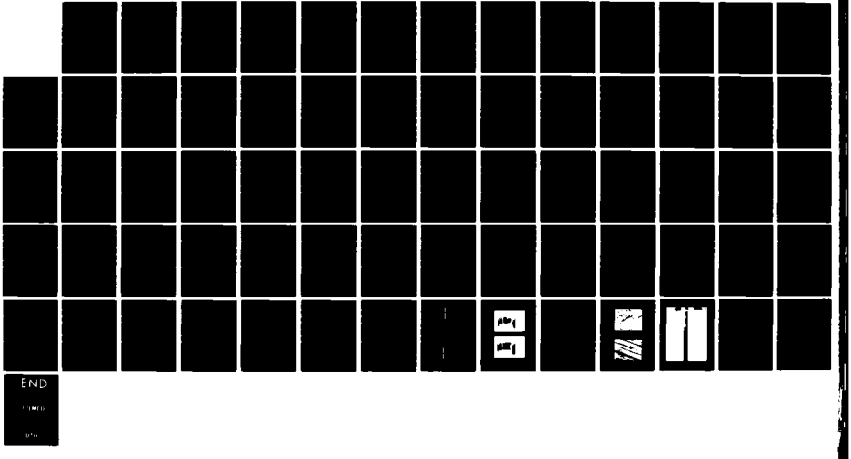

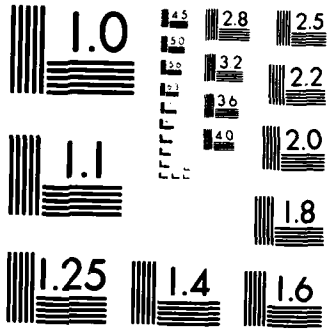

MICROCOPY RESOLUTION TEST CHART
NATIONAL BUREAU OF STANDARDS 1963 A

INTERLAMINAR FRACTURE TOUGHNESS IN RESIN MATRIX COMPOSITES

Lawrence W. Rehfield, Erian A. Armanios and Ambur D. Reddy
School of Aerospace Engineering
Georgia Institute of Technology
Atlanta, Georgia 30332

Annual Scientific Report
1 January 1983 - 14 February 1984
AFOSR Grant No. 83-0056

April 1984

UNCLASSIFIED

SECURITY CLASSIFICATION OF THIS PAGE *(When Data Entered)*

REPORT DOCUMENTATION PAGE	READ INSTRUCTIONS BEFORE COMPLETING FORM
1. REPORT NUMBER **AFOSR-TR- 85-0061**	2. GOVT ACCESSION NO. A150 565
3. RECIPIENT'S CATALOG NUMBER	
4. TITLE *(and Subtitle)* INTERLAMINAR FRACTURE IN RESIN MATRIX COMPOSITES	5. TYPE OF REPORT & PERIOD COVERED Annual 1 January 1983 - 14 February 1984
6. PERFORMING ORG. REPORT NUMBER	
7. AUTHOR(s) Lawrence W. Rehfield, Erian A. Armanios, Ambur D. Reddy	8. CONTRACT OR GRANT NUMBER(s) AFOSR Grant 83-0056
9. PERFORMING ORGANIZATION NAME AND ADDRESS Georgia Institute of Technology School of Aerospace Engineering Atlanta, Georgia 30332	10. PROGRAM ELEMENT, PROJECT, TASK AREA & WORK UNIT NUMBERS 61102F 2307/B2
11. CONTROLLING OFFICE NAME AND ADDRESS Air Force Office of Scientific Research/NA Bolling Air Force Base, DC 20332 - 6448	12. REPORT DATE April 1984
	13. NUMBER OF PAGES 65
14. MONITORING AGENCY NAME & ADDRESS *(if different from Controlling Office)*	15. SECURITY CLASS. *(of this report)* UNCLASSIFIED
	15a. DECLASSIFICATION/DOWNGRADING SCHEDULE

16. DISTRIBUTION STATEMENT *(of this Report)*

Approved for public release; distribution unlimited.

17. DISTRIBUTION STATEMENT *(of the abstract entered in Block 20, if different from Report)*

18. SUPPLEMENTARY NOTES

19. KEY WORDS *(Continue on reverse side if necessary and identify by block number)*

DELAMINATION, INTERLAMINAR FRACTURE, COMPOSITE MATERIALS, COMPOSITE STRUCTURES, FRACTURE TESTING, MODE II FRACTURE, FRACTURE.

20. ABSTRACT *(Continue on reverse side if necessary and identify by block number)*

This annual report summarizes the objectives, accomplishments and proposed new directions of research on mode II interlaminar fracture in resin matrix composites. The work was performed during the period 1 January 1983-14 February 1984. A mode II interlaminar fracture specimen, test and analysis method

DD FORM 1 JAN 73 1473 EDITION OF 1 NOV 65 IS OBSOLETE

UNCLASSIFIED

SECURITY CLASSIFICATION OF THIS PAGE *(When Data Entered)*

for interpreting results have been successfully developed and demonstrated for the AS4/3502 material system. Experimental data have been obtained under both net tensile and compressive loading. Of considerable importance are the findings that (1) the AS4/3502 material system shows increasing resistance to crack growth in tension, (2) interlaminar fracture under compression is a totally unstable process, and (3) tension and compression behaviors are considerably different. The findings and the conclusions that are drawn from them point to new, promising directions for the work. Two new central directions that are suggested involve failure analysis using fractography, radiography and ultrasonic inspection and the quantitative evaluation of mode I suppression technology utilizing the new testing method. Papers, reports and presentations resulting from this research are listed.

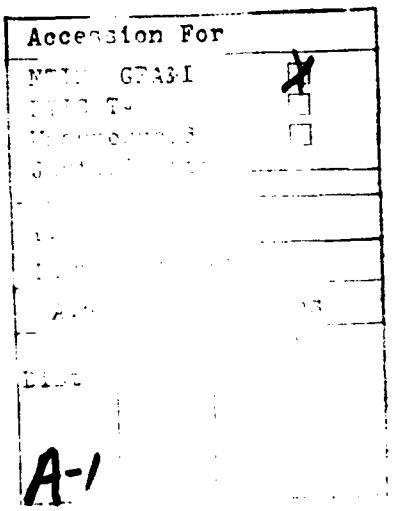

INTRODUCTION

The work described herein was performed at the School of Aerospace Engineering, Georgia Institute of Technology during the period 1 January 1983 - 14 February 1984. Professor Lawrence W. Rehfield was the Principal Investigator. The research objectives are:

1. Develop a mode II interlaminar fracture specimen design and test;
2. Develop efficient means of analyzing and understanding the results; and
3. Design the test so that it may be performed under both net tensile or compressive loading.

All of the above objectives have been met within the first thirteen and one-half month period. In order to accomplish them, it was necessary to develop a suitable method of analysis appropriate to the design process, design and fabricate test specimens and perform definitive experiments.

The experimental results confirm that the specimens and tests perform as designed. Of great importance are the findings that (1) the AS4/3502 material system shows increasing resistance to crack growth in tension, (2) interlaminar fracture under compression is a totally unstable process, and (3) tension and compression behaviors are considerably different. These findings and the logical conclusions that are drawn from them point to new, promising directions for future inquiry and for practical exploitation of the behavioral characteristics that have been found.

SUMMARY OF ACCOMPLISHMENTS

Foundation Provided by Previous Work

The present research in interlaminar fracture had its origin in the development of new structural models under two previous AFOSR grants, 81-0056 and 82-0080, which permitted prediction of interlaminar stresses in composites and nonclassical behavioral characteristics by elementary means. It was natural to harness this potential for design analysis of composite specimens. Earlier analytical work, which was completed and published during the current period and which provided the foundation for the design analysis required in the present research, appears in Accomplishments (1-5, 8). Of importance to the experimental phase of the research are the design analysis method developed in Accomplishment (9), the experimental experience with compression testing in Accomplishment (6) and the experiments on compressed panels with prescribed delaminations reported in Accomplishment (7).

The purpose of citing the above is two-fold: (1) these accomplishments provided the background and the basis for the present research and (2) effort was expended during the present grant period in order to complete them and bring them to publication.

Status of the Research

As indicated in the Introduction, the research objectives were met by developing a suitable method of analysis for use in specimen design, designing and fabricating specimens, and performing the experiments. Much of the work has been clearly and thoroughly described in the manuscript associated with Accomplishment (12h). For this reason, this paper is reproduced in its entirety in the Appendix. Additional information and experimental results are provided, however, in the following sections.

Modeling, Analysis and Design

The key to developing a successful experimental method is an effective design analysis methodology and practical specimen design criteria. The ideal situation is to be able to test under both net tensile and compressive loads, test both statically and in a fatigue spectrum and produce interlaminar cracks in a specimen so that the specimen appears of infinite extent and the notch which serves as the origin of the crack appears isolated.

The analysis methodology evolved over a period of three to four years and has been documented in the invited lecture Accomplishment (10) and Accomplishment (13). A transition has been accomplished from beams to plates[2,5] to composite laminates[1,3] to the present state of sublaminate scale[2,9,11,13]. Originally, a ply-by-ply approach to sublaminate analysis was adopted.[2,11] While extremely effective in the limited context within which it was applied - - - the finite-width free edge specimen in tension, it is cumbersome and appears somewhat impractical for widespread application. Consequently, an approximate engineering approach has been applied in the present work which treats whole sublaminate elements - - - groups of plies - - - as continuous laminates. The novel feature is the fact that the laminate model incorporates physical modes of deformation normally not present in engineering theories - - - transverse shear strain, transverse normal strain and section warping. This laminate model is presented in Accomplishments (1-3).

The refined laminate model, together with the sublaminate approach adopted, are systematically presented in the paper in the Appendix. This design analysis methodology apparently does an adequate job of describing the essential features of the behavior in a simple way[13]. It was used for the specimen design. The details of the design also appear in the Appendix. The methodology is clearly successful as the test specimens behave precisely as designed - - - very clean,

highly regular interlaminar cracks were produced.

The precise limits to this approach are not known, but they may be problem dependent[14]. It may turn out that the features of the global-local scheme of Pagano and Soni[15] are needed in some instances. In this global-local approach, ply-by-ply modeling in the neighborhood of the zone of interest is used (local model), while remote regions are modeled as laminates (global model).

Experimental Method and Results

The experimental method used in testing specimens under net tensile forces is fully described in the Appendix. The compressive test method is similar but also requires the use of a fixture to provide alignment, stabilization of the tabbed ends of the specimen and flat, parallel loading surfaces. Tensile test results appear in the Appendix.

There are two very important findings from the experiments. The first is that under net tensile loading interlaminar fracture is a three stage process - - - initiation, stable growth following a nearly linear resistance curve and a tertiary unstable terminal fracture at a high level of load. The second is that the compressively loaded specimens exhibited absolutely no stable crack growth. Failure occurred in a catastrophic, unstable manner with no warning at a high level of load. Test data for two specimens, one tested in tension and the other in compression, are presented in Figure 1. The loads corresponding to failure by unstable fracture for these specimens are close to the same.

A summary of test results appears in Table I. "SL" denotes a single cracked-lap-shear specimen and "DL" a double cracked-lap-shear specimen, which is the current design. The specimen details are given in the Appendix. Compression is denoted by "C" and tension by "T". The nominal strain is ε, P is the load and G is the energy release rate. While there is some scatter observed in the critical and failure values of these parameters, Figure II in the Appendix shows that the trend

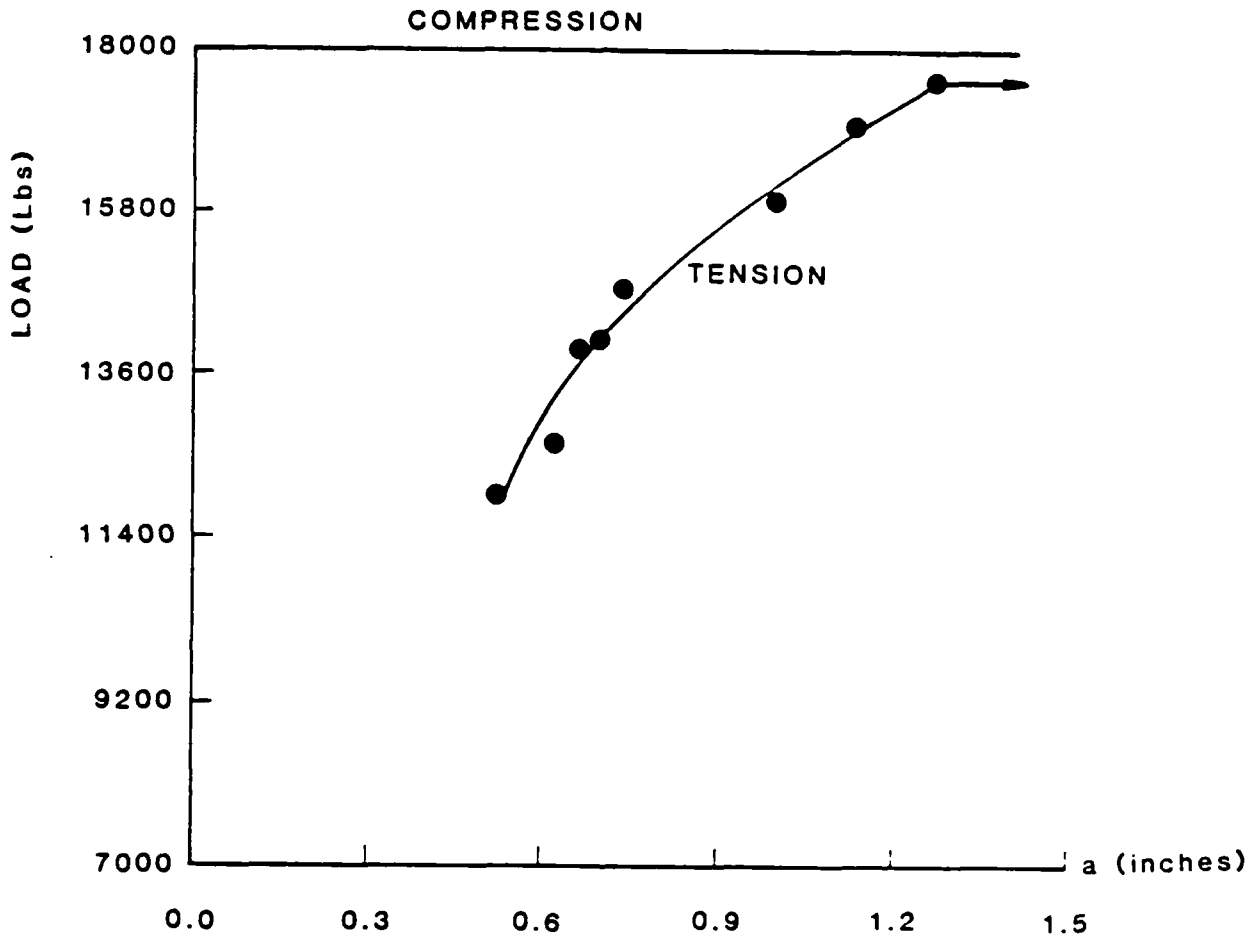

FIGURE 1- TENSION/COMPRESSION TEST DATA

TABLE I

SUMMARY OF TEST RESULTS

SPECIMEN NUMBER	ϵ_c (micro in/in)	ϵ_f	P_c (lbs)	P_f (lbs)	G_c (lb. in/in^2)	G_f
SL-1(C)	5160	5160	18520	18520	4.615	4.615
SL-2(T)	4249	5686	15200	20340	3.186	5.705
SL-3(T)	1768	5064	6320	18100	0.500	4.103
SL-4(T)	3528	4712	12640	16880	2.190	3.906
SL-5(C)	4810	4810	17220	17220	4.055	4.055
SL-6(C)	5228	5228	18600	18600	3.960	3.960
DL-1(T)	3282	4868	12000	17800	2.263	4.979
DL-2(T)	3086	4335	10960	15400	1.964	3.877
DL-3(T)	3101	4156	11180	14980	2.059	3.697
DL-4(C)	3965	3965	14500	14500	3.322	3.322

$E_{effective} = 7.30 \times 10^6$ psi

("c" denotes starting critical value, "f" denotes final or failure)

of increasing resistance to crack growth in tension for the double cracked-lap-shear specimens is consistent and reflects very little scatter. It is very well represented by a linear relationship as indicated in the Appendix.

PRACTICAL IMPLICATIONS OF THE FINDINGS

For the sake of simplicity, assume that the energy release rate for ultimate, unstable interlaminar fracture in tension and compression is the same. This situation is depicted in Figure 2. A mode I resistance curve is depicted as well, which is based upon data supplied by Dr. M.M. Ratwani of the Northrop Corporation[16]. Consider the following: the fundamental difference between the tensile and compressive loading cases for quasi-isotropic layups of AS4/3502 material is a small amount of mode I or crack opening response, estimated at about one percent for ideal geometry and symmetry, in the tension case. It is interesting to speculate that if mode I response is completely suppressed, perhaps tensile and compressive behavior would be similar; that is, sudden, catastrophic, unstable fracture would occur without warning at a high value of load.

There is some evidence which demonstrates that the suppression of mode I response in adhesive joints stops the growth of debonds in tension-dominated fatigue loading[17,18]. This tends to support the above speculation. The well-known effectiveness of stitching, which is a means of suppressing mode I behavior, in stopping the growth of delaminations in laminates[19] and for solving the stiffener "popoff" problem[20] is explained by this line of reasoning.

From a practical standpoint, the implication is that the use of effective mode I suppression technology would permit design to energy release rates of near 4.0 lb-in/in^2 for mode II interlaminar fracture rather than the currently used threshold values near 2.0 lb-in/in^2, at least for graphite/epoxy material systems that behave similarly to AS4/3502. Furthermore, the new mode II test method is an obvious and effective means of evaluating mode I suppression schemes, in addition to its usefulness in providing mode II fracture toughness data.

Considerable effort and resources are being directed toward the development and evaluation of new toughened resins as a way of increasing

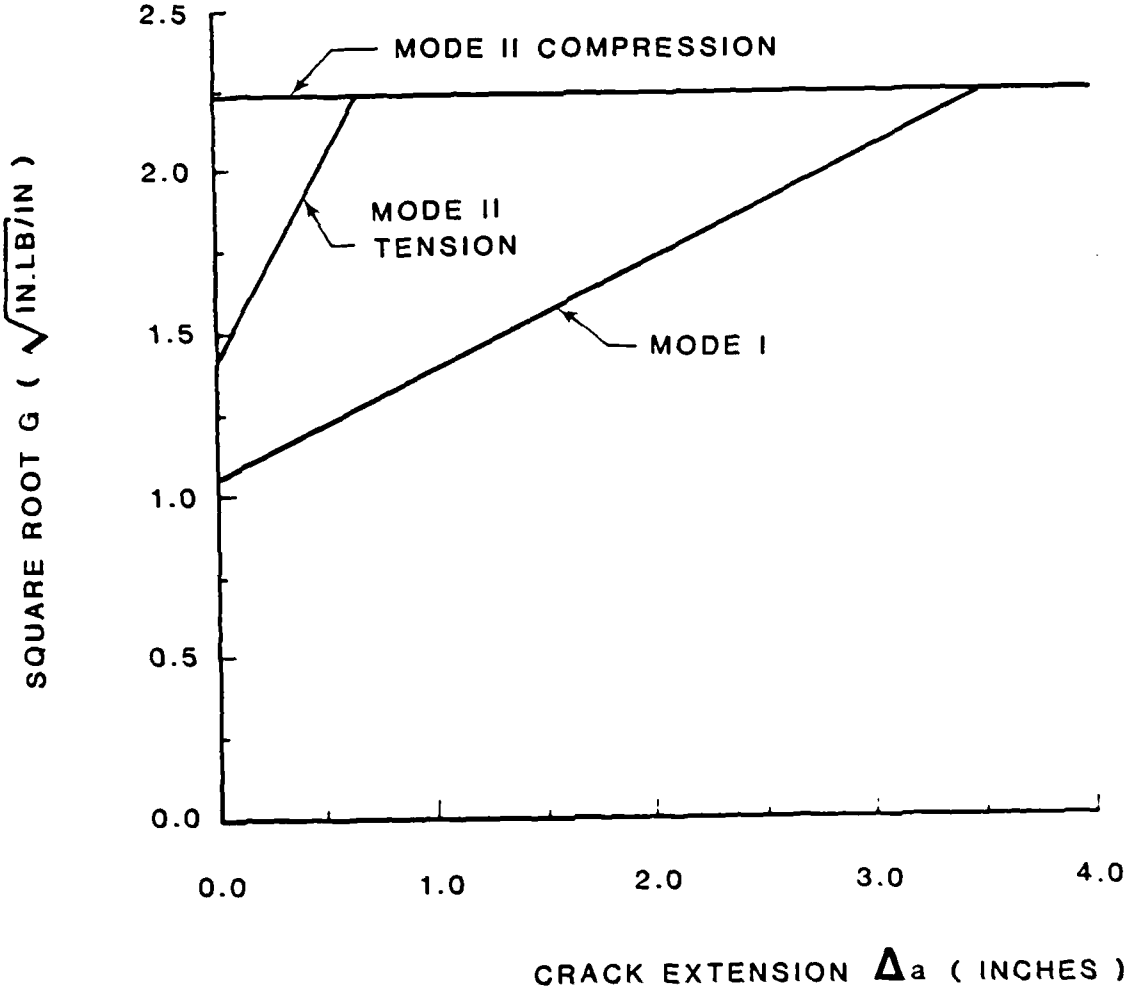

FIGURE 2- COMPARISON OF MODE I & MODE II RESISTANCE CURVES

MODE I AS4/3501-6 COMPOSITE - RATWANI & DEO

MODE II AS4/3502 COMPOSITE - PRESENT

interlaminar fracture toughness in resin matrix composites. Since the mode I double cantilever beam test (DCB test) is simple and well established, it is being used almost exclusively to evaluate the effectiveness of toughened resins[21,22] and other "toughening" schemes[22]. The results of the present research suggest that this practice may be misleading. Mode I data are simply not enough and, if mode I suppression technology is being considered in an application as well, they are the "wrong" information.

Another matter for speculation is whether the unstable fracture processes at high loads can be described by strength-related parameters. It is possible that a failure criterion rather than a crack growth or fracture mechanics-type criterion is more appropriate. A preliminary assessment of this issue has been made by sectioning short beam specimens from undamaged zones of the failed double cracked-lap-shear specimens. These short beam specimens have been tested to failure in three-point bending and the failure loads used to estimate the maximum shear stress by the simple ASTM method. The data appear in Table 2. Also appearing in Table 2 are maximum shear stress values obtained from scaling the maximum shear stress predictions in the Appendix by measured failure loads in the double cracked-lap-shear tests. The agreement among these stress values is striking.

The short beam shear test, therefore, provides definitive information that directly correlates with the mode II fracture test results. It seems to provide a simple, inexpensive means of characterizing the unstable terminal fracture process. While further substantiation of this correlation is desirable, this finding, if true, is of paramount importance. If the speculation about mode I suppression is confirmed, the short beam shear test becomes even more valuable.

These conjectures raise important issues which suggest new means of inquiry

TABLE 2

COMPARISON OF INTERLAMINAR SHEAR DATA

A. MODE II FRACTURE TEST

SPECIMEN	FAILURE LOAD (LB)	MAXIMUM SHEAR STRESS/SHEAR STRENGTH (PSI)
DL-1(T)	17,800	10,193
DL-2(T)	15,400	8,819
DL-3(T)	14,980	8,579
DL-4(C)	14,500	8,304
	MEAN	8,974

B. SHORT BEAM SHEAR TEST

DL-3(T)-1	1,025	7,620
DL-3(T)-2	1,120	8,689
DL-4(C)-1	1,055	7,843
DL-4(C)-2	1,325	9,296
	MEAN	8,362

and new directions for the research that could not be forseen as little as two months ago. Some of these are discussed in the following section.

NEW DIRECTIONS

The results presented are new and contain some surprises. For example, a different mode II specimen and test of the short beam type have been used by Russell[23,24]. On specimens made of ASI/3501-6 graphite/epoxy, he did not find that crack growth resistance increased. In fact, his data could be interpreted as indicating a "negative" resistance. Since the experimental results presented herein are absolutely repeatable for both single and double cracked-lap-shear specimens, this apparent paradox must be resolved. Since Russell's specimen and test are quite similar to the short beam shear test and he states that it is very difficult to control crack growth, the matter may possibly be resolved by a correlation study of the type already conducted for the present material, AS4/3502 graphite/epoxy.

In addition to this matter, the following are some other important questions that are prompted by the new findings:

1. Why does crack growth resistance increase in tension? What is the physical mechanism involved that is acting at or near the crack front?
2. Having identified the above mechanism, can it be enhanced or exploited to create additional benefits?
3. Do other competitive materials behave in the same or a similar manner?
4. Are there any other forms of damage that are occurring in addition to delamination cracking?
5. Is behavior in a fatigue environment similar to static behavior?
6. Do the ply orientations at the lap-strap interface have a marked influence on behavior?
7. Are there thickness effects or can thickness be scaled?

8. Will effective mode I suppression permit damage only by unstable terminal fracture in tension at high load? Alternatively, is the presence of even a little mode I response the cause of the stable crack growth at low tensile loads?
9. Are the unstable fracture processes in tension and compression similar or different?
10. Are the unstable fracture processes similar to fracture of a short beam shear specimen or is the apparent agreement in maximum shear stresses fortuitous?

As more results are obtained and time to reflect upon the new findings is provided, the nature, scope and options for new directions in the research will clearly emerge. At present, it is planned to share and exchange results with Dr. Russell and his associates at Defence Research Establishment Pacific (Victoria, British Columbia) and with Dr. Ratwani's team at Northrop Corporation and to consult with our collaborators at Lockheed-Georgia Company.

The findings and the questions that they provoke prompt us to suggest the following new directions at this juncture:

1. Perform exploratory fatigue tests under both mean tension and mean compression.
2. Study the effect of peel stress or mode I suppression by applying clamping pressure to the lap of a specimen and testing it in static tension. The proposed fixture and test setup for doing this appears in Figure 3.
3. Quantify the effectiveness of a new Lockheed blind stitching method by stitching the lap to the strap of a specimen and testing it in tension.
4. Perform thorough failure analyses using enhanced radiography,

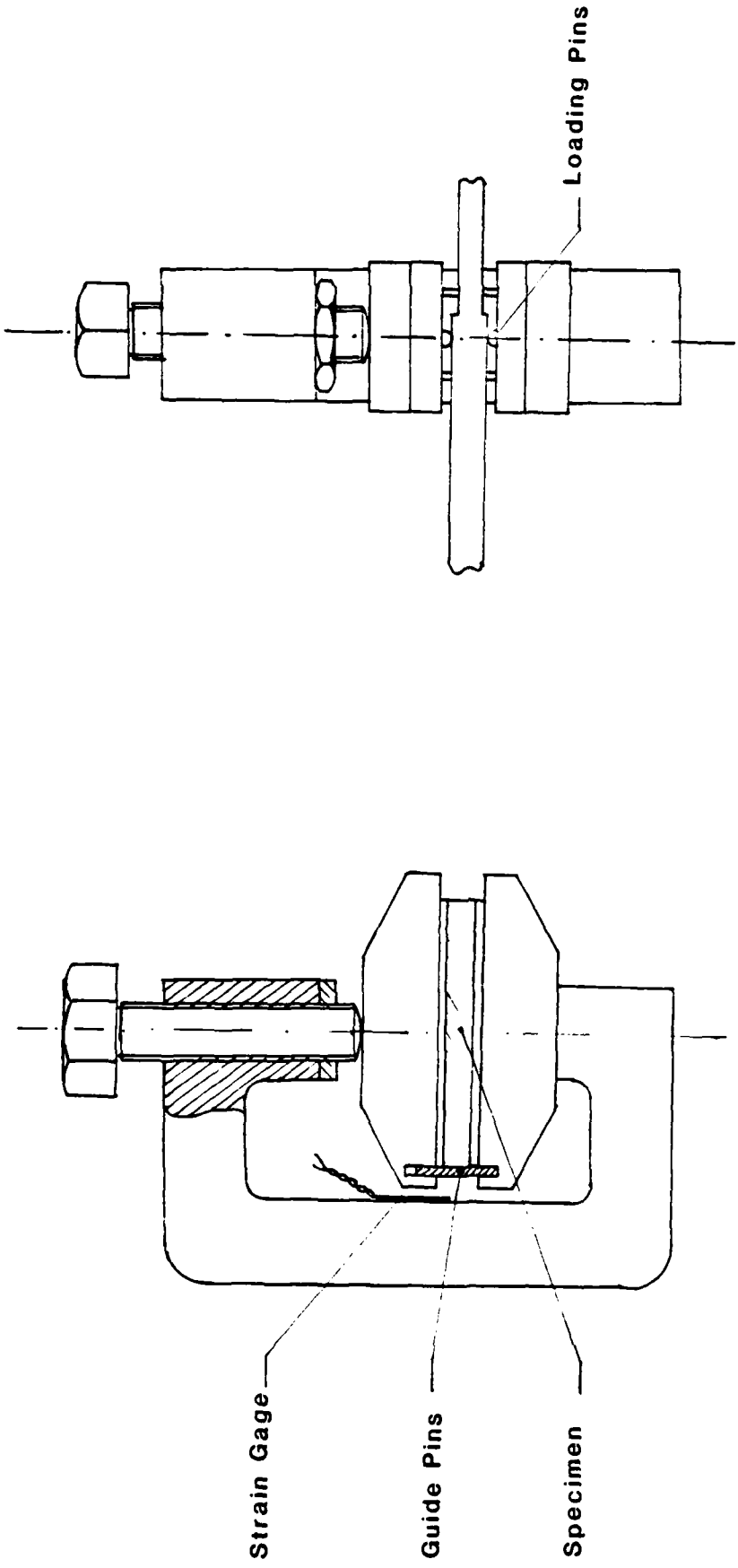

FIGURE 3- FIXTURE FOR MODE I SUPPRESSION STUDIES

ultrasonic scanning, scanning electron microscopy and optical microscopy to determine and characterize the damage states and facilitate isolation of the fracture mechanism(s).

5. Ascertain the influence of material systems, lap-strap interface, and specimen thickness on mode II fracture behavior. A second suggested material is AS4/3501-6, which would permit correlation with mode I and mixed mode data of Northrop Corporation and Russell's data.
6. Study and resolve the apparent paradox surrounding Russell's data and data from the double cracked-lap-shear tests.
7. If mode I suppression is found to be effective in eliminating premature stable crack growth in tension by the methods of items 2 and 3, investigate the effectiveness of softening layers and/or hardening layers introduced in the crack plane.

Item 1 is designed to answer question 5. Items 2, 3 and 7 relate to question 8. Item 4 addresses question 1-6, 9, and 10. Item 5 corresponds to questions 3, 6 and 7. Finally, item 6 will provide answers to questions 3 and 10. When accomplished, these seven items, together with the existing data already obtained, will provide a sound scientific and technological basis for predicting, preventing and managing interlaminar fracture in graphite/epoxy composites.

The two new central directions that are suggested involve failure analysis and mode I suppression technology evaluation. Early in the failure analysis work, the assistance of Mr. Samuel Freeman of the Lockheed-Georgia Company and the equipment provided by a new DoD/AFOSR instrumentation grant will be invaluable. The mode I suppression technology investigations will require the cooperation of Dr. Roy Scruggs of the Manufacturing Branch, Lockheed-Georgia Company. The required cooperation has been pledged.

ACKNOWLEDGMENTS

Numerous persons have contributed to this research over the period of performance by providing advice, exchanging information and responding to questions. A list of them appears in Table 3. Their input has been gratefully received.

TABLE 3

CONTRIBUTORS TO THE RESEARCH

AFOSR:

MAJOR DAVID GLASGOW

GENERAL DYNAMICS:

DICK WILKINS

LOCKHEED-GEORGIA COMPANY:

HARRY ALLEN
SHERRIL BIGGERS
JOHN DICKSON
BERT FERHLE
KRIS KATHIRESAN

NORTHROP CORPORATION:

RAVI DEO
MOHAN RATWANI

AFML:

JAMES WHITNEY

NASA LANGLEY RESEARCH CENTER:

WOLF ELBER
STEVEN JOHNSON
KEVIN O'BRIEN
BLAND STEIN
JOHN WHITCOMB

ACCOMPLISHMENTS

Publications

1. Rehfield, L.W., and Valisetty, R.R., "A Comprehensive Theory for Planar Bending of Composite Laminates," presented at the Symposium on Advances and Trends in Structural and Solid Mechanics, Computers and Structures, Vol. 16, No. 1-4, 1983, pp. 441-447.

2. Valisetty, R.R., "Bending of Beams, Plates and Laminates: Refined Theories and Comparative Studies," Ph.D. Thesis, Georgia Institute of Technology, March 1983.

3. Valisetty, R.R., and Rehfield, L.W., "A Theory for Stress Analysis of Composite Laminates," Proceedings of the 24th AIAA Structures, Structural Dynamics and Materials Conference, May 1983, pp. 144-153. Also submitted to the AIAA Journal.

4. Yehezkely, O., and Rehfield, L.W., "A New, Comprehensive Theory for Bending and Buckling of Stiffened Plates," Israel Journal of Technology, Vol. 21, August 1983.

5. Rehfield, L.W., and Valisetty, R.R., "A Simple, Rfined Theory for Bending and Stretching of Homogeneous Plates," AIAA Journal, Vol. 22, No. 1, January 1984, pp. 90-95.

6. Reddy, A.D., Rehfield, L.W., Haag, R.S., and Widman, C., "Compressive Buckling Behavior of Graphite/Epoxy Isogrid Wide Columns with Progressive Damage," appears in Compression Testing of Homogeneous Materials and Composites, ASTM STP 808, edited by R. Chait and R. Paperino, 1983, pp. 187-199.

7. Reddy, A.D., Rehfield, L.W. and Haag, R.S., "Effect of Large Delaminations on the Compressive Postbuckling Behavior of Laminated Composite Panels," Proceedings of the Sixth Conference on Fibrous Composites in Structural Design, Report AMMRC MS 83-2, Army Materials and Mechanics Research Center, November 1983, pp. VI-41 to VI-51.

8. Rehfield, L.W., Prucz, J., and Murthy, P.L.N., "Influence of Hygrothermal Conditioning on the Compressive Buckling of Graphite/Epoxy Structures," Journal of the American Helicopter Society, Vol. 29, No. 2, April 1984.

Presentations

9. Rehfield, L.W. and Armanios, E.A., "Analysis of Behavior of Fibrous Composite Compression Specimens," Second U.S. - Japan Symposium on Composite Materials, NASA Langley Research Center, Hampton, VA, June 6-8, 1983. To appear in Proceedings of the Second U.S./Japan Conference on Composite Materials, edited by J. Vinson, an ASTM STP Volume.

Presentations Continued:

10. Rehfield, L.W., "Innovations in Modeling for Conventional and Composite Structures," Invited Lecture, Army Materials and Mechanics Research Center, Watertown, MA, 28 July 1983.

11. Valisetty, R. R., and Rehfield, L.W., "A New Approach to Interlaminar Stress Analysis," ASTM Symposium on Delamination and Debonding of Materials, Pittsburgh, PA, 9-10 November 1983. To appear in Delamination and Debonding of Materials, edited by W.S. Johnson, an ASTM STP Volume.

12. Armanios, E. A., Rehfield, L.W., and Reddy, A.D., "Design Analysis and Testing for Mode II Interlaminar Fracture of Composites," presented at

    a. Northrop Corporation, Hawthorne, CA, 27 February 1984.

    b. Hughes Helicopter, Inc., Culver City, CA, 1 March 1984.

    c. Army Aeromechanics Laboratory, Ames Research Center, Moffett Field, CA, 5 March 1984.

    d. Invited Lecture, Seminar on Matrix Resins for Composites, United Nations Industrial Development Organization and Dept. of Science and Technology, Government of India, Indian Institute of Technology, Delhi, India, 12-14 March 1984.

    e. *Messerschmitt-Bölkow-Blohm, Helicopter Division*, Munich, West Germany, 19 March 1984.

    f. Army Applied Technology Laboratory, Fort Eustis, VA, 27 March 1984.

    g. NASA Langley Research Center, Hampton, VA, 28 March 1984.

    h. ASTM Symposium on Composite Materials: Testing and Design, Philadelphia, PA, 2-4 April 1984. To be published in Composite Materials: Testing and Design, edited by J.M. Whitney, an ASTM STP Volume.

    i. Boeing Vertol Company, Philadelphia, PA, 4 April 1984.

    j. Sikorsky Aircraft, Stratford, CT, 5 April 1984.

    k. Lockheed-Georgia Company, Marietta, GA, 16 April 1984.

13. Rehfield, L.W., Armanios, E.A., and Valisetty, R.R., "Simplified Sublaminate Analysis of Composites and Applications," Symposium on Advances and Trends in Structures and Dynamics, Washington, D.C., 22-24 October 1984, to appear in Computers and Structures

REFERENCES

14. Pagano, N.J., Private Communication, AFWAL/MLBM, WPAFB, OH, February 1984.

15. Pagano, N.J. and Soni, S.R., "Global Local Laminate Variational Model," International Journal of Solids and Structures, Vol. 19, No. 3, pp. 207-228, 1983.

16. Ratwani, M.M., Private Communication, Northrop Corporation, Hawthorne, CA, March 1984.

17. Everett, R.A., Jr.: The Significance of Peel Stresses in Cyclic Debonding. M.S. Thesis, Old Dominion University, 1980.

18. Dattaguru, B., Everett, R.A., Jr., Whitcomb, J.D. and Johnson, W. S., "Geometrically Nonlinear Analysis of Adhesively Bonded Joints," NASA TM-84562, September 1982.

19. Garrett, R.A., "The Effect of Manufacturing and Service-Induced Defects on the Strength of Aircraft Composite Structures," presented at the ASTM Symposium on Composite Materials: Testing and Design, Philadelphia, PA, 2-4 April 1984. to be published in Composite Materials: Testing and Design, edited by J.M. Whitney, an ASTM STP Volume.

20. Williams, J., and Starnes, J.H., Jr., Private Communication, NASA Langley Research Center, Hampton, VA, March 1984.

21. Ashizawa, M., "Improving Damage Tolerance of Laminated Composites Through the Use of New Tough Resins," Proceedings of the Sixth Conference on Fibrous Composites in Structural Design, Report AMMRC MS 83-2, Army Materials and Mechanics Research Center, November 1983, pp. IV-21 to IV-45.

22. Browning, C.E., and Schwartz, H.S., "Delamination Resistant Concepts," presented at the ASTM Symposium on Composite Materials: Testing and Design, Philadelphia, PA, 2-4 April 1984. To be published in Composite Materials: Testing and Design, edited by J.M. Whitney, an ASTM STP Volume.

23. Russell, A.J., and Street, K.N., "Factors Affecting the Interlaminar Fracture Energy of Graphite/Epoxy Laminates," Progress in Science and Engineering of Composites, edited by T. Hayashi, K. Kawata and S. Umekawa, ICCM-IV, Tokyo, 1982, pp. 279-286.

24. Russell, A.J., Private Communication, Philadelphia, PA, April 1984.

APPENDIX

Presented at the Seventh Symposium on Composite Materials: Testing and Design, Philadelphia, Pennsylvania, April 2-4, 1984

DESIGN ANALYSIS AND TESTING FOR MODE II INTERLAMINAR FRACTURE OF COMPOSITES

E. A. Armanios, L.W. Rehfield and A. D. Reddy*

ABSTRACT: This paper presents the design analysis and results of an experimental program that was conducted to evaluate the Mode II interlaminar fracture behavior of a resin matrix composite material system. A double cracked-lap-shear specimen was designed utilizing a simple, new analysis method and tested in static tension. The specimen was made of AS4/3502 graphite/epoxy material with a $(\pm 45, 0, 90)_{12s}$ quasi-isotropic balanced symmetric layup. The lap interface studied was at $\pm 45^{o}$ orientations to the loading direction. The crack growth during testing was monitored by observing the isochromatic fringes in photoelastic coatings mounted on the two lap surfaces. Preliminary results indicate that the fracture behavior follows a resistance curve.

KEY WORDS: composite materials, fiber-reinforced composites, composite structures, graphite-epoxy, crack propagation, fracture, delamination, scanning electron microscopy, test methods

---

* Graduate Research Assistant, Professor and Senior Research Engineer, respectively.

INTRODUCTION

Laminated composite structures exhibit a number of different failure modes. These include fiber-matrix debonding within individual layers, delamination or separation of the layers, transverse cracks through one or more layers and fiber fracture. A complex state of stress with steep gradients exists in regions near free edges, ply terminations, cutouts, holes and voids. These sites often initiate interlaminar delamination cracks due to high local interlaminar shear and normal stresses. Delamination is observed to be one of the most common damage modes in composites. A material characteristic that could be used to determine resistance to delamination growth is the strain energy release rate G. Investigations on the strain energy release rate associated with Mode I fracture have been reported by several authors [1-6].

The most popular test to determine Mode II interlaminar fracture toughness is based on the use of a single cracked-lap-shear type specimen [7]. It requires extensive nonlinear numerical calculations to analyze and interpret the test results. This is not a satisfactory situation. The objective of the present work is to develop a simpler approach where the Mode II contribution to fracture is predominant and to be able to analyze and interpret the results by elementary methods.

The heart of the approach is a simple, new analysis method which permits the rapidly varying interlaminar stresses to be determined by elementary means. Extensive numerical computations are thus avoided and the results are obtained in closed form. The parameters governing the behavior are easily identified. The specimen selected for test is a symmetric double cracked-lap-shear type specimen with end tabs as shown in Figure 1. The layup is selected to produce balanced symmetric specimens with differently oriented interface plies at the lap/strap

junction. This also minimizes the nesting effect that would occur if similar plies were used at the interface. This specimen is designed to be tested in both tension and compression. The geometry of the lap, strap and tabs is designed to precipitate crack growth in the gage section. Overall dimensions of the specimen are determined by the boundary layer effects from tab ends and from the lap/strap junction. Interaction among the local stresses in the above regions is avoided. The lengths of lap and strap regions are selected so as to provide an adequate crack length to be monitored and to prevent overall buckling of the specimen. Symmetric crack growth is enhanced by choosing a large specimen thickness and by strict control of manufacturing quality.

The overall objective of this work is to systematically examine this specimen behavior in static tension and compression. This paper, however, summarizes the design analysis, manufacturing and tension testing only. The resistance curve developed from the test data is also presented.

OVERVIEW OF ANALYSIS APPROACH

The present analysis models are based on the theory developed in Reference 8. This theory includes transverse shear strain, transverse normal strain and section warping effects. These effects, which are ignored by classical theories, can be significant in structures constructed of modern composite materials. For laminated composite structures, the theory will be applied on a ply-by-ply basis or to a group of plies . . . sublaminates . . . as if they are homogeneous bodies in equilibrium. Interfacial stresses are initially unknown. Enforcement of continuity conditions at interfaces and boundary conditions in an overall sense leads to a solution for these stresses. A complete development of the anlaytical model is given in the Appendix.

A simplification can be made by neglecting overall bending of the sublaminates. This model will be referred to as the "sublaminate membrane

model". The basic equations for this model are derived from the Appendix equations by neglecting the underlined terms and the sublaminate moment terms. For a sublaminate in a plane strain situation, these equations encompass the following main categories:

Overall Equilibrium:

$$N^k_{,x} + t_2^k - t_1^k = 0 \tag{1}$$

$$Q^k_{,x} + p_2^k - p_1^k = 0 \tag{2}$$

$$\frac{h^k}{2}(t_2^k + t_1^k) - Q^k = 0 \tag{3}$$

The normal and transverse shear stress resultants of the kth element are N^k and Q^k, respectively. The interfacial shear stresses on the top and bottom surfaces of the kth element are t_2 and t_1. The interfacial transverse normal stresses are p_2 and p_1. The thickness of the kth element is h^k. Superscript "k", which identifies the element, will be dropped in the subsequent equations for convenience.

Constitutive Relation:

$$N = h E_{11} u_{,x} + h \nu_{13} r - \frac{h^2}{12} \nu_{13} N_{,xx} \tag{4}$$

where

$$r = \frac{1}{2}(p_2 + p_1) \tag{5}$$

The elastic modulus associated with the x direction is E_{11}. Poisson's ratio is ν_{13}. The average axial displacement is $\tilde{u}$.

Stress Distribution:

$$\sigma_{xx}(x, z) = \frac{N}{h} + \frac{h}{24}\left(\frac{E_{11}}{G_{13}} - 2\nu_{13}\right)\left(1 - \frac{12z^2}{h^2}\right)N_{,xx} \qquad (6)$$

$$\sigma_{xz}(x, z) = -\frac{z}{h}N_{,x} + \frac{Q}{h} \qquad (7)$$

$$\sigma_{zz}(x, z) = r - \frac{h}{8}\left(1 - \frac{4z^2}{h^2}\right)N_{,xx} - \frac{z}{h}Q_{,x} \qquad (8)$$

The stress components follow the usual elasticity notations. The transverse shear modulus is G_{13}.

Displacement Distribution:

$$w(x, z) = \tilde{w} - \frac{\nu_{13}}{E_{11}}\frac{z}{h}N \qquad (9)$$

$$u(x, z) = \tilde{u} - z\tilde{w}_{,x} + \frac{1}{2hE_{11}}\left[\frac{h^2}{12}\left(\frac{E_{11}}{G_{13}} - \nu_{13}\right)\left(1 - \frac{12z^2}{h^2}\right)N_{,x} + 2\frac{E_{11}}{G_{13}}zQ\right] \qquad (10)$$

$$\tilde{\phi} = -\tilde{w}_{,x} + \frac{1}{hG_{13}}Q \qquad (11)$$

The average transverse displacement is $\tilde{w}$, and the average section rotation is $\tilde{\phi}$.

The boundary conditions appropriate to this model are limited to extensional behavior. N or $\tilde{u}$ must be prescribed at the element ends. The interlaminar continuity condition (A-2) and the traction boundary conditions at the extreme upper and lower surfaces of the laminate must be imposed, and they remain unchanged for this model.

Bending effects at the sublaminate level are considered in the sublaminate bending model. For this model, the equations used are those given in the Appendix with the underlined terms neglected. The boundary conditions appropriate to this

model are limited to extensional and bending behavior. N or $\tilde{u}$ and M or $\tilde{\phi}$ must be prescribed at the sublaminate ends. Transverse force and displacement conditions cannot be independently prescribed at this level of approximation. The interlaminar continuity conditions (A-2) and the traction boundary conditions at the extreme upper and lower surfaces of the laminate remain unchanged.

In order to verify the accuracy of the present formulations, a comparison with a finite element solution is presented. The double-lap specimen shown in Figure 1 is subjected to uniform compression. Due to symmetry, only one half of the problem is analyzed. The finite element simulation of the problem is shown in Figure 3. The element used is a constant strain four-node rectangular element. The total number of elements used is 3700. The finite element code used is the Engineering Analysis Language (EAL). A comparison of the stress distribution at the interface between the lap and the strap is shown in Figures 4a and 4b for a specimen made of T300/5208 graphite/epoxy with +45/-45 interface at the lap/strap junction. The number of plies in the lap region is 8 and in the strap is 32. The lap length is L. In the constant strain finite element as well as in the sublaminate membrane model, the shear stress-free boundary condition at the end of the lap region cannot be satisfied. In the sublaminate bending model, this condition is satisfied.

Delamination crack growth is usually characterized by the strain-energy release rate. For linear, elastic material behavior [10], and the proposed specimen geometries

$$G = P^2(dc/da)/2b \qquad (12)$$

where P is the applied load, c is the specimen compliance, a is the crack length and b is the specimen width. The critical strain energy release rate, G_c, is obtained by substituting the critical load P_c for P in Equation (12). In this context, the load

required to cause a crack extension is defined as critical load. An expression for the compliance as a function of crack length can be determined by using Equations (1) - (5), (9) and (10), along with the appropriate boundary and loading conditions. The three components of the strain energy release rate G_I, G_{II} and G_{III} associated with the opening mode, the forward shearing mode, and the tearing mode can be calculated by using the stress field predicted from the proposed models and the crack-closure method [11]. Since the present specimen is assumed to be under plane strain condition, Mode III effects are not present. The design of the specimen will be based on the predictions of the sublaminate bending model.

SPECIMEN DESIGN

In order to determine the overall dimensions of the specimen, a parametric study has been conducted in which the material properties of the specimen are those of AS4/3502 graphite/epoxy. Woven fiber glass end tabs are utilized. The number of plies in the lap and strap regions is varied. Three interfaces at the lap/strap junction are considered, namely +45/-45, 0/90 and 0/45. The level of model used does not permit a distinction for different stacking sequences or interface plies. The optimum number of plies and specimen dimensions were determined based on the following:

(1). Preventing overall buckling.

(2). Initiating a crack at lap/strap juncture first.

(3). Providing an adequate length to monitor crack growth.

(4). Ensuring no interaction between stress boundary layers at the tab/step, tab/lap, tab/strap and the lap/strap regions.

(5). Minimizing Mode I contribution to crack growth.

A crack will start first at the lap/strap juncture if the dimensions of the lap, strap and tabs are determined so as to produce the higher stress intensity at the lap/strap

juncture. This is illustrated in Figure 5 by comparing the interlaminar shear stress distribution at the lap/strap interface with the tab/lap and tab/strap distributions. The interface length is L. Moreover, interaction of stress boundary layers at the tab/lap and the lap/strap regions is eliminated if the distance between these regions is adequate for the stress boundary layers to decay to an allowable value. This situation is illustrated in Figure 6. The axial stress distribution through the depth of the specimen strap is plotted. The strap length is a_1 and the strap half thickness is t. The depth coordinate z is measured from the strap middle-plane. For the stress to decay to within five percent of the uniform stress value in the lap/strap region and the gauge section, the decay length is $0.26a_1$ and $0.19a_1$ from the lap end.

The final design is shown in Figure 7. The number of plies in the lap and strap region is 8 and 32, respectively. The lap/strap body interface is +45/-45. The lap layup is $[\pm 45, 0, 90]_s$ and the strap layup is $[\pm 45, 0, 90]_{4s}$. A single panel was fabricated by the Lockheed-Georgia Company and inspected for quality using standard aerospace industry practice before sectioning into ten test specimens. During layup, a folded Kapton film was placed at the end of the lap/strap interface to initiate a delamination under subsequent loading.

The available strain energy release rate for the designed specimen can be calculated using Equation (15). A simplification can be made by neglecting the stresses in the cracked portion of the lap with crack growth. For this situation, the compliance of the specimen consists of two parts. The first is a linear function of the crack length. This contribution is similar to the strength of materials extensional model reported in Reference 7. The second, an exponential function of the crack length, can be regarded as a refinement added to the first term. For the specimen geometry and material used, the refined term is found to be negligible for

practical range of crack lengths. This situation is illustrated in Figure 8. The energy release rate is plotted against crack growth from zero to 10 times the strap half thickness t. For that range of crack growth, the ply membrane and the ply bending predictions are within one percent of the strength of materials prediction labelled "Extension" in this figure.

For this specimen, the Mode II contribution to fracture is predominant as the ratio of the Mode I to Mode II strain-energy-release rates (G_I/G_{II}) is 0.01.

EXPERIMENTAL PROCEDURE AND PRELIMINARY RESULTS

The static tension tests on the double cracked-lap-shear specimens were performed on a displacement controlled Baldwin screw-type testing machine. The specimens were carefully positioned and the tab ends were tightly held between serrated grips. Two techniques were tried to measure the crack growth in the specimen. The first method involved visual observation of the cracks on the white painted (typewriter correction fluid) specimen edge [7]. In the second method, a sheet of photoelastic material was bonded on each of the surfaces of the specimen lap portion [12]. Isochromatic fringes develop at the crack front as a result of the high strain gradient in that vicinity when the specimen is loaded. These fringes were tracked through the analyzer of a reflection polariscope to locate the crack front. By comparison, the edge cracks observed from the first method did not correspond to the averaged crack length of the curved crack front observed by the second method. This was because the crack fronts were irregular regardless of the care exercised in initially aligning the specimen. Hence, the first method was considered unreliable and was abandoned. The second method was used on all the specimens due to its simple and direct nature in monitoring the crack front. Also, the isochromatic fringes served to check initial uniformity of the applied load on the specimen. The specimen was also instrumented with a custom-built, linear

variable differential transformer (LVDT) displacement transducer based extensometer to measure its compliance.

The specimen was loaded continuously and the front and back cracks were followed through separate polariscopes. At a certain critical load, the first threshold of the crack growth occurred at the lap/strap juncture and it grew beyond the Kapton film. With crack growth, the specimen stiffness reduces and hence the load drops in a controlled displacement machine. Loading was stopped whenever crack growth was observed and the extent of propagation was recorded together with the load. The crack growth was initially stable but intermittent on the two fronts with one crack trying to maintain parity with the other. During this phase, crack growth was possible only under increasing load. The crack front was not planar and it curved forward at the specimen edges. The specimen failure occurred finally with both the cracks growing in an unstable manner. The load value corresponding to this event was recorded. In general, there was no crack wandering through the plies. Pictures of the isochromatic fringes before the initial crack propagation and during the stable crack growth phase are presented in Figures 9 and 10. The crack growth data, taken at five locations along the width of the specimen and from both the front and back faces, was averaged to obtain a resultant crack length corresponding to each load. To eliminate the edge effects, crack length values at the edges were discarded in the averaging process. Altogether, three specimens were tested and the data is presented in Figure 11. Numbers 1, 2 and 3 in this figure correspond to data points from specimens 1, 2 and 3, respectively. The data were plotted together as the specimens were generated from the same parent panel.

The failed specimens were sectioned and the fracture surfaces were observed under a scanning electron microscope. Typical photomicrographs of a fracture surface immediately after the Kapton film in the stable region and in the

unstable region of crack growth are presented in Figures 12a and 12b respectively.

DISCUSSION

The load vs. crack growth data appears in Figure 11. The data shows that there is a consistent increase in the critical load with crack length. A linear least squares fit through this data is also plotted in Figure 11. Although the fit corresponding to the least standard deviation is parabolic, its improvement over the linear fit is only 2.5 percent. The simplicity and advantages of the linear fit is preferred over the parabolic fit. The multiple correlation coefficient, r^2, corresponding to the linear fit is 0.926. The linear fit equation is

$$P_c = 50,590 + 18,359\ \Delta a \quad (N, \Delta a \text{ in cm})$$
$$P_c = 11,373 + 10,483\ \Delta a \quad (lb, \Delta a \text{ in inches}) \tag{13}$$

where P_c is the critical load corresponding to a crack extension a. The data from future additional tests will be included to enhance confidence in the above fit.

As outlined in the previous section and illustrated in Figure 8, the $\frac{dc}{da}$ values can be considered independent of crack length and will be computed using the strength of materials approach (Reference 7). This also checks with the dc/da values computed from the experimental specimen compliance data. From this and Equation (12), it follows that the critical strain energy release rate (G_c) is proportional to the square of the critical load only. Figure 11 can also be regarded as a plot of scaled $\sqrt{G_c}$ vs crack length which is similar to a crack growth resistance curve.

The substitution of Equation (13) into (12) gives the following fit between $\sqrt{G_c}$ and crack extension Δa

$$\sqrt{G_c} = 19.19 + 692.94\ \Delta a \qquad (\sqrt{J/m},\ \Delta a \text{ in m})$$

$$\sqrt{G_c} = 1.45 + 1.33\ \Delta a \qquad (\sqrt{\text{in lb/in}},\ \Delta a \text{ in inches}) \qquad (14)$$

There are three phases in the resistance curve. A starting region corresponding to the onset of crack growth, an intermediate region corresponding to stable crack growth and a final or failure region of unstable crack growth. The fit shown in Figure 11 and represented in Equations (13) and (14) describes the stable crack growth region.

The results on the three specimens are summarized in Table I. The critical loads that initiated the crack growth beyond the Kapton film and the corresponding energy release rates are listed. Based on results from the analytical model, G_{IIc} is computed as 0.99 times G_{Tc}. The total critical strain energy release rate is G_{Tc}. The small amount of scatter in the observed critical load data may be attributable to the design and testing approach chosen. The symmetry in the specimen virtually eliminates nonlinear effects and the $\pm$ 45° interface minimized nesting and the resulting crack wandering. Observation of the crack front by means of the photoelastic coating provided complete characterization across the width of the specimen and helped accurately determine the initial and subsequent crack growths with loading. This situation is different compared to the problems encountered in single cracked-lap-shear specimen testing.

Preliminary tests on 48 ply ($\pm$ 45, 0, 90) quasi-isotropic layup (8 plies in the lap) single cracked-lap-shear specimens made of AS4/3502 graphite/epoxy material exhibited the following problems:

(1) The first crack did not always initiate at the lap/strap juncture;

(2) Multiple, isolated cracks occurred and sometimes grew in opposite directions;

(3) The crack at lap/strap juncture wandered.

Figure 13 presents a typical failed single cracked-lap-shear specimen depicting the

above problems. these factors might contribute to the data scatter appreciably. Test results performed on three single cracked-lap-shear specimens also indicated that the fracture behavior follows a resistance curve. A summary of test results on the three specimens is presented in Table 2. Plots of critical load vs crack length based on the data presented in Reference 7 for a single cracked-lap-shear specimen, are shown in Figures 14 and 15. Two material systems were tested and five panels of ten specimens each were fabricated from each material. Figure 14 corresponds to the data presented in Table 5 of Reference 7 on two specimens made of ASI/3506-1 graphite/epoxy material system and in a room temperature dry environment. They are numbered 1 and 2. Figure 15 presents the data listed in Table 7 of Reference 7 on three specimens made of T300-6K/V378A graphite/bismaleimide material system and tested also in a room temperature dry environment. They are numbered 1, 2 and 3. The author presented and analyzed the data of each specimen separately. An alternative way is to look at the specimen data produced at a given temperature/moisture condition together. The wide scatter in the data and the concern expressed by the author may be attributable to the specimen used and the crack tracking method (based on edge crack information only) employed.

From Figure 12a, the fracture surface appears to have predominantly high matrix deformation with lacerated resin bands. These are believed to correspond to the stop-start regions of the load dependent crack fronts observed. The unstable crack growth region shown in Figure 12b is characterized by a relatively smooth surface with fiber pull out and breakage. Striations are observed throughout the fiber pull-out region.

CONCLUSIONS

A double cracked-lap-shear specimen has been designed using simple analytical models. These models provided good estimates for stresses compared to

the finite element model used. This has been tested in static tension to determine the Mode II interlaminar fracture behavior. The preliminary data generated are consistent and provide similar behavioral trends on the specimens tested.

The specimen behaved as designed and the crack started at the lap/strap interface and grew in an intermittent but stable fashion with increasing applied load. This stable crack growth phase was followed by an unstable one which resulted in the disbonding of the laps from the strap to the vicinity of the grips. All these events were followed by observing the isochromatic fringes in photoelastic coatings bonded to the two lap portions. There was no crack wandering at the lap/strap juncture. The scatter in the critical load data at initial cracking was small. This demonstrates the advantages of using a double cracked-lap-shear specimen.

The preliminary results provided delamination growth resistance curves for the AS4/3502 graphite/epoxy material system with a $\pm$ 45^{o} step/body interface. The average value obtained for the Mode II strain energy release rate, G_{IIc}, corresponding to the onset of crack growth is 363.3 J/m^2 (2.074 in lb/in^2).

ACKNOWLEDGEMENTS

This work was supported by the U.S. Air Force Office of Scientific Research under Grant AFOSR-83-0056. This support is gratefully acknowledged. Specimens used in this test program were manufactured and supplied by the Lockheed-Georgia Company. We acknowledge Dr. Kris Kathiresan for his cooperation. The finite element code EAL was provided by Engineering Information Systems Inc., Saratoga, California; this assistance is also gratefully acknowledged.

REFERENCES

1. Wilkins, et al., "Characterizing Delamination Growth in Graphite Epoxy," ASTM STP 775, 1982.

2. Whitney, J.M., Browning, L.E. and Hougsteden, W., "A Double Cantilever Beam Test for Characterizing Mode I Delamination of Composite Materials," Journal of Referenced Plastics and Composites, October 1982.

3. Nicholls, D.J. and Gallagher, J.P., "Determination of G_{Ic} in Angle-Ply Composites Using a Double Cantilever Beam Test," Journal of Reinforced Plastics and Composites, January 1983.

4. Whitney, J.M. and Browning, C.G., "Materials Characterization for Matrix Dominated Failure Modes," ASTM Conference on Effects of Defects, San Francisco, December 1982.

5. Wang, S.S., "Delamination Crack Growth in Unidirectional Fiber-Reinforced Composites Under Static and Cyclic Loading," Composite Materials: Testing and Design (Fifth Conference), ASTM STP 674, American Society for Testing and Materials, 1980.

6. O'Brien, T.K., "Characterization of Delamination Onset and Growth in a Composite Laminate," Damage in Composite Materials: Basic Mechanism, Accumulation, Tolerance and Characterization, ASTM STP 775, 1982.

7. Wilkins, D.J., "A Comparison of the Delamination and Environmental Resistance of a Graphite-Epoxy and a Graphite-Bismaleimide," Technical Report, NAV-GD-0037, September, 1981.

8. Rehfield, L.W. and Murthy, P.L.N., "Toward a New Engineering Theory of Bending: Fundamentals," AIAA Journal, Vol. 20, No. 5, May 1982.

9. Valisetty, R.R., "Bending of Beams, Plates and Laminates: Refined Theories and Comparative Studies," Ph.D. Thesis, Georgia Institute of Technology, March 1983.

10. Paris, P.C. and Sih, G.C. in Fracture Toughness Testing, ASTM STP 381, 1970.

11. Eshelby, J.C., Stress Analysis of Cracks, ISI Publication 121, 1968.

12. Roderick, G.L., Everett, R.A., and Crews, J.H., Jr. in Fatigue of Composite Materials, ASTM STP 569, American Society for Testing and Materials, 1975, pp. 295-306.

13. Murthy, P.L.N., "A New Engineering Theory of Planar Bending and Applications," Ph.D. Thesis, Georgia Institute of Technology, Dec. 1981.

14. Rehfield, L.W. and Valisetty, R.R., "A Simple, Refined Theory for Bending and Stretching of Homogeneous Plates," AIAA Journal, Vol. 22, No. 1, January 1984.

15. Rehfield, L.W. and Valisetty, R.R., "A Comprehensive Theory for Planar Bending of Composite Laminates," Computers and Structures, Vol. 16, No. 1-4, 1983, pp. 441-447.

16. Valisetty, R.R. and Rehfield, L.W., "A Theory for Stress Analysis of Composite Laminates," AIAA Paper 83-0833-CP, Presented at the 24th AIAA/ASME/ASCE/AHS Structures, Structural Dynamics and Materials Conference, Lake Tahoe, Nevada, May 2-4, 1983.

TABLE I. SUMMARY OF EXPERIMENTAL DATA ON DOUBLE CRACKED-LAP-SHEAR SPECIMENS

SPECIMEN NUMBER	P_{cr}		$(dc/da) \times 10^8$		G_{Tcr}		G_{IIcr}	
	(N)	(LB)	(m/J)	(IN/LB IN)	(J/m^2)	(IN LB /IN^2)	(J/m^2)	(IN LB/IN^2)
1	53379	(12000)	1.411	(6.277)	396.7	(2.265)	392.7	(2.242)
2	48753	(10960)	1.470	(6.540)	343.8	(1.963)	340.3	(1.943)
3	49731	(11180)	1.481	(6.590)	360.6	(2.059)	357.0	(2.038)

TABLE 2. SUMMARY OF EXPERIMENTAL DATA ON SINGLE CRACKED-LAP-SHEAR SPECIMENS

SPECIMEN NUMBER	P_{cr}		$(dc/da) \times 10^8$		G_{Tcr}	
	(N)	(LB)	(m/J)	(IN/LB IN)	(J/m^2)	(IN LB/IN^2)
1	67613	(15200)	1.240	(5.515)	558.0	(3.186)
2	28113	(6320)	1.125	(5.003)	87.6	(0.500)
3	56226	(12640)	1.230	(5.472)	383.4	(2.189)

LIST OF FIGURES

APPENDIX

Development of the Analytical Model

Foundations of the Model

The development that follows is based upon the fundamental assumption that the statically equivalent stresses obtained from classical engineering theory can be used to estimate the transverse shear and normal strains ignored in the classical theory. All subsequent results follow from this premise. These strain estimates permit a suitable displacement field to be determined, which further leads to improved stresses. This approach has been thoroughly documented and evaluated for beams [8], plates [14], and composite laminates [15, 16] by comparisons with exact solutions (when available), finite element solutions, demonstrations of correspondence with other established theories and order of magnitude error investigations [9, 13].

In the present work, models appropriated to individual plies of a laminate or groups of plies . . . sublaminates . . . are developed using the same fundamental logic and assumptions. The development is restricted to static plane stress states. The same results can be used, however, in a plane strain situation by a proper transformation of the elastic constants. This restriction is not intrinsic to the present development. It allows the presentation of essential features in a simple way without confronting the additional complexities of fully three-dimensional behavior.

Statically Equivalent Stress Field

Consider a laminate made of N perfectly bonded layers or plies, each ply having a plane of material symmetry parallel to the plane of the laminate. Let "k" denote a particular ply that is singled out for study. The ply thickness is h^k. Let

x^k and y^k represent the coordinates in the mid-plane of the ply. The interlaminar stresses σ_{zz} and σ_{xz} at the top of the ply are denoted by p_2 and t_2, respectively, while the corresponding stresses at the bottom of the ply are designated as p_1 and t_1. Notation and sign convention appear in Figure 2.

The equilibrium equations that are valid within each ply are

$$(\sigma_{xx,x} + \sigma_{xz,z})^k = 0$$

$$(\sigma_{zx,x} + \sigma_{zz,z})^k = 0 \qquad \text{(A-1)}$$

The usual convention and notation are followed: σ_{xx} is the axial stress, σ_{zz} is the transverse normal stress, and σ_{xz} the transverse shear stress. Superscript "k" signifies that each variable within the parenthesis is associated with the k-th ply.

The above equations are supplemented by interlaminar conditions which ensure reciprocity of tractions and continuity of displacements at the interfaces between plies. At the interface between the k^{th} and the $(k-1)^{th}$ plies, they are

$$t_1^k = t_2^{k-1}$$

$$p_1^k = p_2^{k-1}$$

$$u^k(x^k, -\frac{h^k}{2}) = u^{k-1}(x^{k-1}, \frac{h^{k-1}}{2})$$

$$w^k(x^k, -\frac{h^k}{2}) = w^{k-1}(x^{k-1}, \frac{h^{k-1}}{2}) \qquad \text{(A-2)}$$

The axial component of the displacement is u^k and the lateral component is w^k. In addition, traction boundary conditions are normally specified at the extreme upper and lower surfaces of the laminate. At the boundaries corresponding to constant

values of x, the laminate sections, boundary conditions will be enforced in an overall sense as is commonly done in engineering theories of bending and stretching.

Overall equations of equilibrium in terms of force and moment resultants may be derived by appropriate integration of Equations (A-1). They are

$$N^k_{,x} + t_2^k - t_1^k = 0$$

$$Q^k_{,x} + p_2^k - p_1^k = 0$$

$$M^k_{,x} - Q^k + \frac{h^k}{2}(t_2^k + t_1^k) = 0 \qquad \text{(A-3)}$$

The force, moment and transverse shear stress resultants of the k-th ply are N^k, M^k and Q^k, respectively. These bear the classical definitions.

$$(N^k, M^k, Q^k) = \int_{-h^k/2}^{h^k/2} (\sigma_{xx}, z\sigma_{xx}, \sigma_{xz})^k \, dz \qquad \text{(A-4)}$$

Superscript "k", which identifies the ply, will be dropped in the subsequent equations for convenience.

According to classical theory, the stresses that satisfy equilibrium equations (A-2) and interlaminar stress boundary conditions at the top and bottom surfaces of each ply are

$$\sigma_{xx} = \frac{N}{h} + \frac{12M}{h^3} z \qquad \text{(A-5)}$$

$$\sigma_{xz} = \frac{z}{h}(t_2 - t_1) + \frac{3}{2h}\left(1 - \frac{4z^2}{h^2}\right)Q - \frac{1}{4}\left(1 - \frac{12z^2}{h^2}\right)(t_2 + t_1) \qquad \text{(A-6)}$$

$$\sigma_{zz} = \frac{1}{2}(p_2 + p_1) + \frac{h}{8}(1 - \frac{4z^2}{h^2})(t_2 - t_1)_{,x} + \frac{3z}{2h}(1 - \frac{4z^2}{3h^2})(p_2 - p_1) + \frac{z}{4}(1 - \frac{4z^2}{h^2})(t_2 + t_1)_{,x}$$

(A-7)

The following contractions which denote the sum and difference of interlaminar stresses are introduced for convenience

$$n = t_2 - t_1$$

$$m = \frac{h}{2}(t_2 + t_1)$$

$$q = p_2 - p_1$$

$$r = \frac{1}{2}(p_2 + p_1)$$

(A-8)

n can be regarded as an effective distributed axial force, m an effective distributed moment, q an effective lateral pressure and r a mean flatwise tensile stress.

The stresses given in Equations (A-5) through (A-7), although not exact, are statically equivalent to the applied surface loadings. They will be used subsequently to develop approximations for the displacement components.

Kinematics

The central assumption in the present development is that the statically equivalent stresses in Equations (A-5) through (A-7) can be used to estimate the transverse normal strain and transverse shear strain. This is not a kinematic assumption, but an assumption regarding stresses.

The development will be carried out for orthotropic materials with principal material directions corresponding to axes of the ply. The appropriate form of Hooke's law for plane stress is

$$\varepsilon_{xx} = S_{11}\sigma_{xx} + S_{13}\sigma_{zz} \tag{A-9}$$

$$\varepsilon_{zz} = S_{13}\sigma_{xx} + \underline{S_{33}\sigma_{zz}} \tag{A-10}$$

$$\gamma_{xz} = S_{55}\sigma_{xz} \tag{A-11}$$

ε_{xx}, ε_{zz}, γ_{xz} are the axial strain, transverse normal strain, and transverse shear strain, respectively. The S-terms are flexibilities; in terms of engineering constants, they are

$$S_{11} = 1/E_{11}$$

$$S_{13} = -\nu_{13}/E_{11}$$

$$S_{33} = 1/E_{33}$$

$$S_{55} = 1/G_{13} \tag{A-12}$$

E_{11} and E_{33} are elastic moduli associated with the x and z directions. ν_{13} is Poisson's ratio and G_{13} is the transverse shear modulus. The underlined term in Equation (A-10) represents the influence of the transverse normal stress in estimating the transverse normal strain. The same convention will be followed throughout the development to identify this type of contribution. Its effect upon the derived equations will be discussed later.

The strain components are related to the displacement components by the following strain displacement relations:

$$u_{,x} = \varepsilon_{xx}$$

$$w_{,z} = \varepsilon_{zz}$$

$$u_{,z} + w_{,x} = \gamma_{xz} \tag{A-13}$$

Equations (A-5), (A-7), (A-10) and (A-13) permit the transverse normal strain to be approximated as

$$w_{,z} \cong S_{13}\left(\frac{N}{h} + \frac{12M}{h^3} z\right) + S_{33}\left[r + \frac{h}{8}\left(1 - \frac{4z^2}{h^2}\right)n_{,x} + \frac{3z}{2h}\left(1 - \frac{4z^2}{3h^2}\right) q + \frac{z}{2h}\left(1 - \frac{4z^2}{h^2}\right) m_{,x}\right] \tag{A-14}$$

Integration of this equation results in the following expression for the lateral displacement component w:

$$w = W(x) + S_{13} z \left(\frac{N}{h} + \frac{12M}{h^3} z\right) + \frac{1}{2} S_{33}\, z\left[2r + \frac{h}{4}\left(1 - \frac{4z^2}{3h^2}\right)n_{,x} + \frac{3z}{2h}\left(1 - \frac{2z^2}{3h^2}\right)q + \frac{z}{2h}\left(1 - \frac{2z^2}{h^2}\right) m_{,x}\right] \tag{A-15}$$

$W(x)$ is the lateral deflection of the ply axis $z = 0$.

The axial component of displacement u can be estimated as follows. Equations (A-11) and (A-13) permit $u_{,z}$ to be expressed as

$$u_{,z} = S_{55}\sigma_{xz} - w_{,x} \tag{A-16}$$

Substitution of (A-6) and (A-15) into Equation (A-16) and subsequent integration results in

$$u = U(x) - zW(x) + \frac{z^2}{2h} S_{55}\, Sn + \frac{3z}{2h}\left(1 - \frac{4z^2}{3h^2} S\right) S_{55}Q - \frac{z}{2h}\left(1 - \frac{4z^2}{h^2} S\right)S_{55}\, m$$

$$-\frac{1}{4} S_{33} z^2 \left[2r_{,x} + \frac{h}{4}\left(1 - \frac{2z^2}{3h^2}\right) n_{,xx} + \frac{z}{h}\left(1 - \frac{2z^2}{5h^2}\right) q_{,x} + \frac{z}{3h}\left(1 - \frac{6z^2}{5h^2}\right) m_{,xx}\right] \qquad \text{(A-17)}$$

where

$$S = 1 + S_{13}/S_{55} \qquad \text{(A-18)}$$

U(x) is the axial deflection at the ply axis.

The static displacement field is completely described by Equations (A-15), (A-17) and (A-18). This approximate displacement field was determined by estimating precisely the strains that are ignored in classical theory. U and W, the axis displacement components, emerge as natural kinematic variables. The kinematic compatibility equations of continuum theory are not satisfied exactly by this displacement field. The objective, however, is not rigor but a consistent, reliable engineering theory which features high accuracy together with simplicity. The approximations made are consistent with the other inherent approximations introduced [9, 13].

Refined Axial Stress

The axial stress in the ply is usually large and of the greatest importance. An accurate knowledge of it is essential in practical applications. A refined estimate that improves Equation (A-5) is central to the theoretical improvements that are sought.

Equations (A-7), (A-9), and (A-17) can be utilized to produce a refined axial stress expression

$$\sigma_{xx} = \frac{1}{S_{11}}\, u_{,x} - S_{13}\sigma_{zz})$$

$$= \frac{1}{S_{11}}\Bigg\{U_{,x} - z\,W_{,xx} - S_{13}r - \frac{h}{8}S_{13}\left[1 - \frac{4z^2}{h^2}\left(2 + \frac{S_{55}}{S_{13}}\right)\right]n_{,x}$$

$$- \frac{S_{13}z}{2h}\left[1 + \frac{S_{55}}{S_{13}} - \frac{4z^2}{h^2}\left(2 + \frac{S_{55}}{S_{13}}\right)\right]m_{,x} - \frac{3z}{2h}S_{13}\left[1 + \frac{S_{55}}{S_{13}} - \frac{4z^2}{3h^2}\left(2 + \frac{S_{55}}{S_{13}}\right)\right]q$$

$$\underline{-\frac{1}{4}S_{33}z^2\left[2r_{,xx} + \frac{h}{4}\left(1 - \frac{2z^2}{3h^2}\right)n_{,xxx} + \frac{z}{h}\left(1 - \frac{2z^2}{5h^2}\right)q_{,xx} + \frac{z}{3h}\left(1 - \frac{6z^2}{5h^2}\right)m_{,xxx}\right]}\Bigg\}$$

(A-19)

Relationships for the axial force and moment resultants are obtained by using Equations (A-4) and (A-19). The results are

$$N = \frac{h}{S_{11}}\left[U_{,x} - S_{13}r - \frac{h}{24}S_{13}\left(1 - \frac{S_{55}}{S_{13}}\right)n_{,x} \underline{- \frac{h^2}{16}S_{33}\left(\frac{2}{3}r_{,xx} + \frac{3h}{40}n_{,xxx}\right)}\right]$$

$$M = \frac{h^3}{12S_{11}}\left[-W_{,xx} - \frac{3}{10h}S_{13}\left(3 + 4\frac{S_{55}}{S_{13}}\right)q + \frac{S_{13}}{10h}\left(1 - 2\frac{S_{55}}{S_{13}}\right)m_{,x} \underline{- \frac{h}{1120}S_{33}\left(39\,q_{,xx} + 11m_{,xxx}\right)}\right]$$

(A-20)

Equations (A-20) permit Equation (A-19) to be rewritten as

$$\sigma_{xx} = \frac{N}{h} + \frac{12M}{h^3}z - \alpha\left[\frac{h}{12}\left(1 - \frac{12z^2}{h^2}\right)n_{,x} + \frac{3z}{5h}\left(1 - \frac{20z^2}{3h^2}\right)\left(q + m_{,x}\right)\right]$$

$$\underline{+ \frac{h^2}{16}\frac{S_{33}}{S_{11}}\left\{\frac{2}{3}\left(1 - \frac{12z^2}{h^2}\right)r_{,xx} + \frac{3h}{40}\left[1 - \frac{40z^2}{3h^2}\left(1 - \frac{2z^2}{3h^2}\right)\right]n_{,xxx}\right.}$$

$$\underline{\left. + \frac{39z}{70h}\left[1 - \frac{280}{39}\frac{z^2}{h^2}\left(1 - \frac{2z^2}{5h^2}\right)\right]q_{,xx} + \frac{11z}{70h}\left[1 - \frac{280}{33}\frac{z^2}{h^2}\left(1 - \frac{6z^2}{5h^2}\right)\right]m_{,xxx}\right\}}$$

(A-21)

The parameter α is $(S_{55} + 2S_{13})/2S_{11}$; it is unity for an isotropic material.

It has been shown [9, 13] that the transverse normal and shear stress distributions which are consistent with the refined axial stress distribution (A-21) are those given by the classical expression in Equations (A-6) and (A-7).

Summary

The governing equation for the present model can be summarized now. They encompass four categories. Overall-type equations consist of the equilibrium equations (A-3) and the constitutive equations (A-20). In addition, two sets of equations provide the distributions of stresses and displacements throughout the ply. The first set for stresses consists of Equations (A-21), (A-6), and (A-7). The second for displacements is composed of Equations (A-15) and (A-17).

Considerable simplification is achieved if the underlined terms in the governing equations are neglected. This is equivalent to neglecting the influence of the transverse normal stress in estimating the transverse normal strain as indicated in Equation (A-10). The implications of this approximation and its accuracy are discussed in Reference 9.

In the place of axis-related kinematic variables, averaged variables can also be used. These are defined as

$$\tilde{u} = \int_{-h/2}^{h/2} \frac{u}{h}\, dz$$

$$\tilde{w} = \int_{-h/2}^{h/2} \frac{w}{h}\, dz \qquad \text{(A-22)}$$

In addition to the averaged kinematic variables in Equations (A-22), it is convenient to introduce an intermediate kinematic variable that is related to ply

section rotation. This is selected to be the mean rotation of the ply section.

$$\tilde{\phi} = \int_{-h/2}^{h/2} \frac{u_{,z}}{h} dz = \frac{1}{h}\left[u(x, h/2) - u(x, -h/2)\right] \qquad \text{(A-23)}$$

The above collection of equations requires the specification of boundary conditions at specified values of x. There are three boundary conditions per end. It is usual in an engineering theory to prescribe N or $\tilde{u}$, Q or $\tilde{w}$, and M or $\tilde{\phi}$. Ply-axis kinematic variables can also be used in specifying kinematic boundary conditions. The modeling of boundary restraint conditions in classical theory is straightforward since the displacement varies linearly through the entire thickness. The situation is more complex here. Experience with the use of the equations and specific study of the sensitivity of predictions to boundary restraint modeling are required. The corresponding problem for homogeneous structures is discussed in References [8, 14].

For convenience, the constitutive relations, along with the stress and displacement distributions in terms of averaged kinematic variables and derivatives of resultant force and moment, are listed below.

Constitutive relations:

$$N = \frac{h}{S_{11}}\left[\tilde{u}_{,x} - S_{13}r + \frac{h}{12} S_{13} N_{,xx} + \underline{\frac{7h^3}{2880}\alpha S_{13} N_{,xxxx}}\right]$$

$$M = \frac{h^3}{12S_{11}}\left[-\tilde{w}_{,xx} + \frac{1}{h}(S_{13} + S_{55})Q_{,x} + \frac{2\alpha}{5h} S_{11} M_{,xx} - \underline{\frac{S_{33}h}{60} Q_{,xxx} - \frac{S_{33}h}{10}\left(\frac{1}{21} - \frac{\alpha S_{13}}{8S_{33}}\right)M_{,xxxx}}\right] \qquad \text{(A-24)}$$

Displacement distribution:

$$w = \tilde{w} + \frac{z}{h} S_{13} N - \frac{S_{13}}{2h}\left(1 - \frac{12z^2}{h^2}\right)M$$

$$+ \frac{S_{33}h}{2}\left[\frac{2z}{h}r - \frac{z}{4}\left(1 - \frac{4z^2}{3h^2}\right) N_{,xx} + \left(\frac{1}{12} - \frac{z^2}{h^2}\right) Q_{,x} + \left(\frac{7}{240} - \frac{z^2}{2h^2} + \frac{z^4}{h^4}\right) M_{,xx}\right]$$

$$u = \tilde{u} - z\tilde{w}_{,x} + \frac{z}{h} S_{55} Q + \frac{1}{2}(S_{55} + S_{13})\left[\frac{h}{12}\left(1 - \frac{12z^2}{h^2}\right) N_{,x} + \frac{z}{h}\left(1 - \frac{4z^2}{h^2}\right)M_{,x}\right]$$

$$+ \frac{h^2 S_{33}}{48}\left[2\left(1 - \frac{12z^2}{h^2}\right)r_{,x} - 3h\left(\frac{3}{40} - \frac{z^2}{h^2} + \frac{2z^4}{3h^4}\right) N_{,xxx} - \frac{2z}{h}\left(1 - \frac{4z^2}{h^2}\right)Q_{,xx}\right.$$

$$\left. - \frac{z}{h}\left(\frac{7}{10} - \frac{4z^2}{h^2} + \frac{24}{5}\frac{z^4}{h^4}\right) M_{,xxx}\right]$$

(A-25)

Stress distribution

$$\sigma_{xx} = \frac{N}{h} + \frac{12M}{h^3} z + \alpha\left[\frac{h}{12}\left(1 - \frac{12z^2}{h^2}\right)N_{,xx} + \frac{3z}{5h}\left(1 - \frac{20}{3}\frac{z^2}{h^2}\right)M_{,xx}\right]$$

$$+ \frac{S_{33}}{16S_{11}} h^2\left[\frac{2}{3}\left(1 - \frac{12z^2}{h^2}\right)r_{,xx} - \frac{3h}{40}\left(1 - \frac{40}{3}\frac{z^2}{h^2} + \frac{80}{9}\frac{z^4}{h^4}\right) N_{,xxxx} - \frac{2z}{5h}\left(1 - \frac{20}{3}\frac{z^2}{h^2}\right)Q_{,xxx}\right.$$

$$\left. - \frac{11z}{70h}\left(1 - \frac{280}{33}\frac{z^2}{h^2} + \frac{112}{11}\frac{z^4}{h^4}\right)M_{,xxxx}\right]$$

$$\sigma_{xz} = -\frac{z}{h} N_{,x} + \frac{Q}{h} + \frac{1}{2h}\left(1 - \frac{12z^2}{h^2}\right)M_{,x}$$

$$\sigma_{zz} = r - \frac{h}{8}\left(1 - \frac{4z^2}{h^2}\right) N_{,xx} - \frac{z}{h} Q_{,x} - \frac{z}{2h}\left(1 - \frac{4z^2}{h^2}\right)M_{,xx}$$

(A-26)

Method of Solution

The above equations are to be applied to individual plies of a laminate or to groups of plies. . . . sublaminates . . . as needed to analyze a situation producing significant interlaminar stresses. The following are the solution steps in terms of averaged kinematic variables:

1. Divide the laminate into elements according to geometry and loading condition. The element length is selected such that within the element the geometry and loading are continuous as is commonly done in engineering theories of bending and stretching. Elements and/or sublaminates are characterized by their effective extensional or flexural moduli as appropriate.
2. The displacements, resultant force and moment, and interlaminar stresses in each element are governed by the equilibrium equations (A-3), the constitutive relations (A-20) and the displacement distributions (A-15) and (A-17). Write these equations for each element in the analysis model.
3. Apply interlaminar continuity conditions (A-2) and enforce tractions or displacements conditions at the extreme upper and lower surfaces of the laminate.
4. Solve the system of coupled ordinary differential equations for the elements variables.
5. Enforce the boundary conditions at constant values of x, the laminate sections, as well continuity requirements between element ends as is commonly done in engineering theories of bending and stretching in order to find the values of the arbitrary constants resulting from the solution in step 4.
6. Determine through-thickness stress and displacement distributions from the element variables using Equations (A-26) and (A-25), respectively.

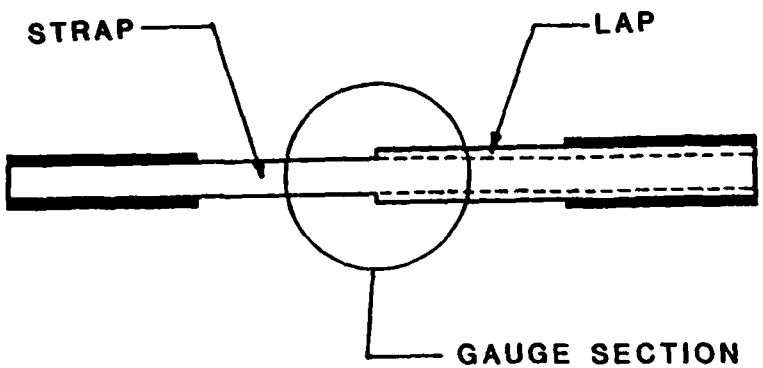

FIG. 1

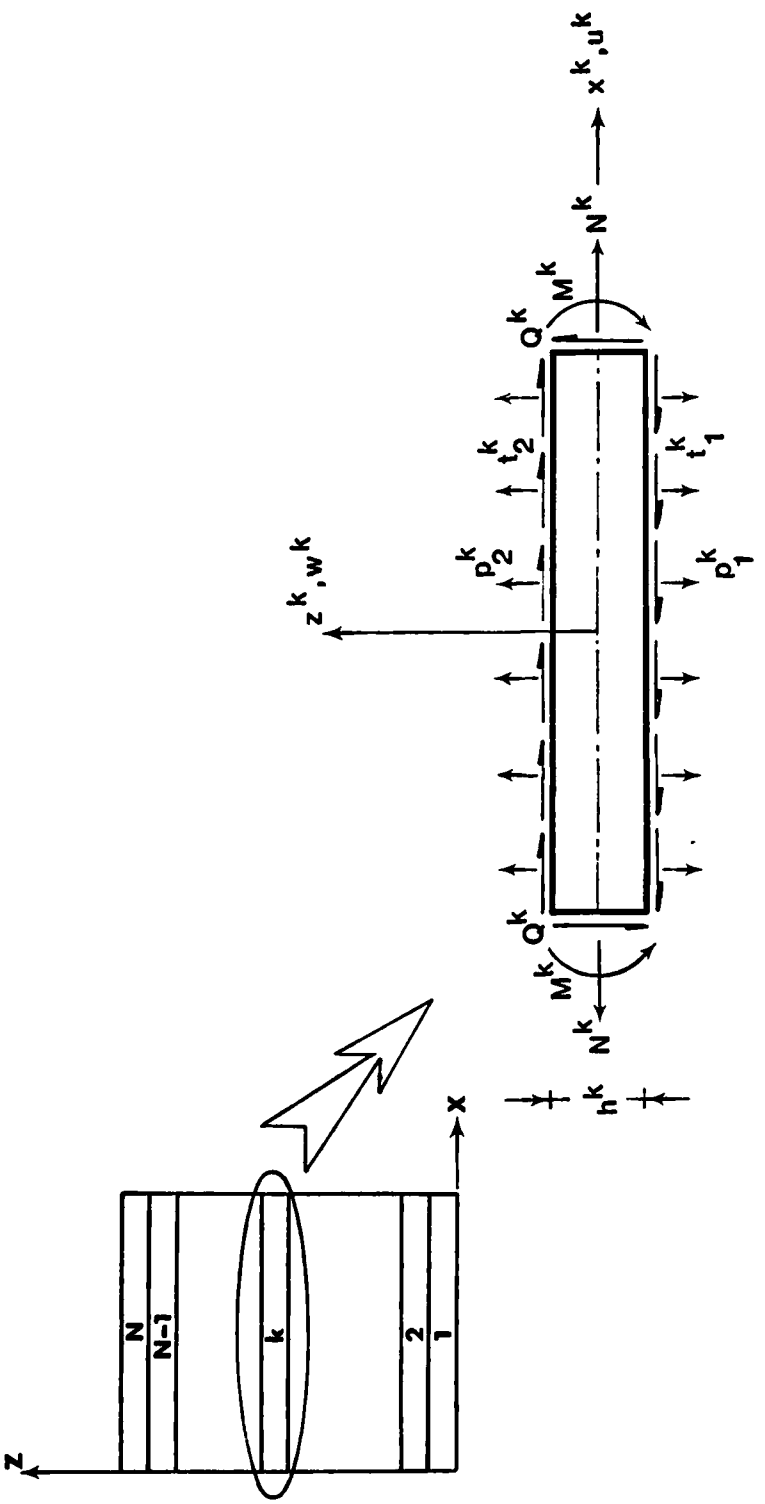

FIG. 2

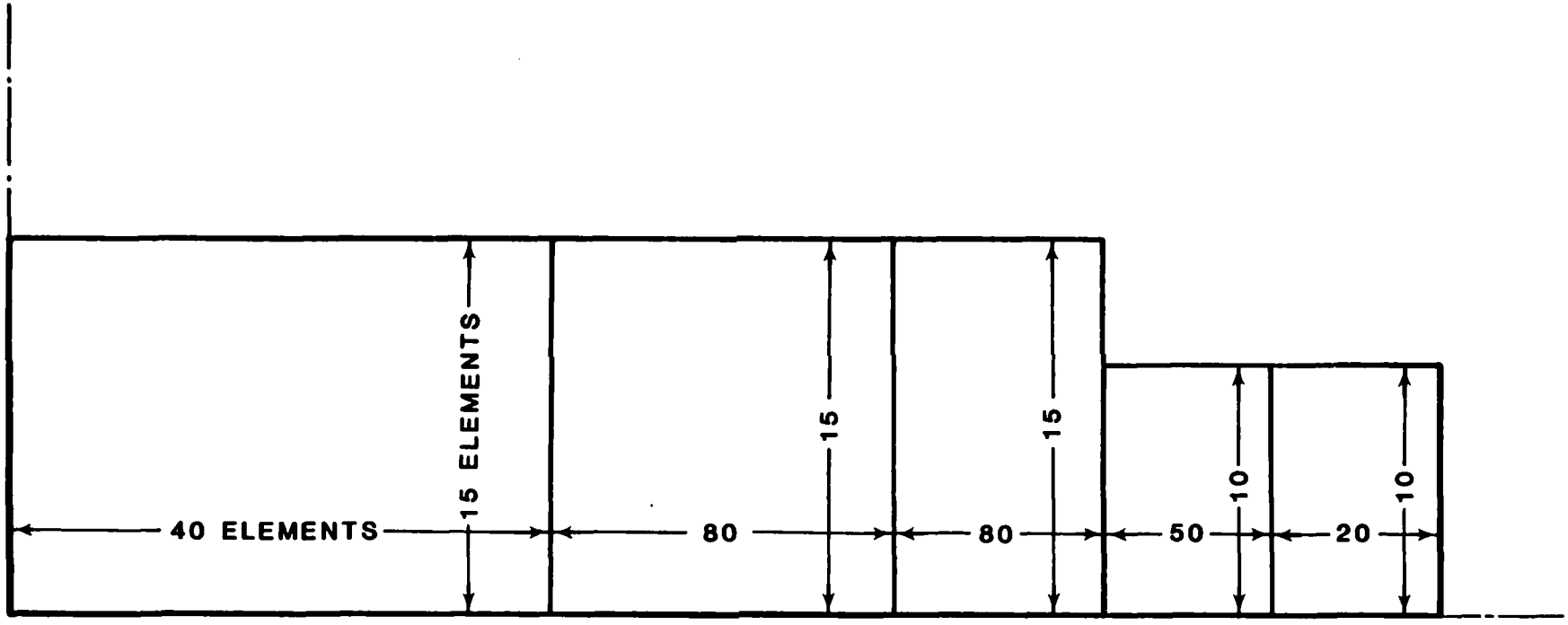

TOTAL NUMBER OF ELEMENTS : 3700

FIG. 3

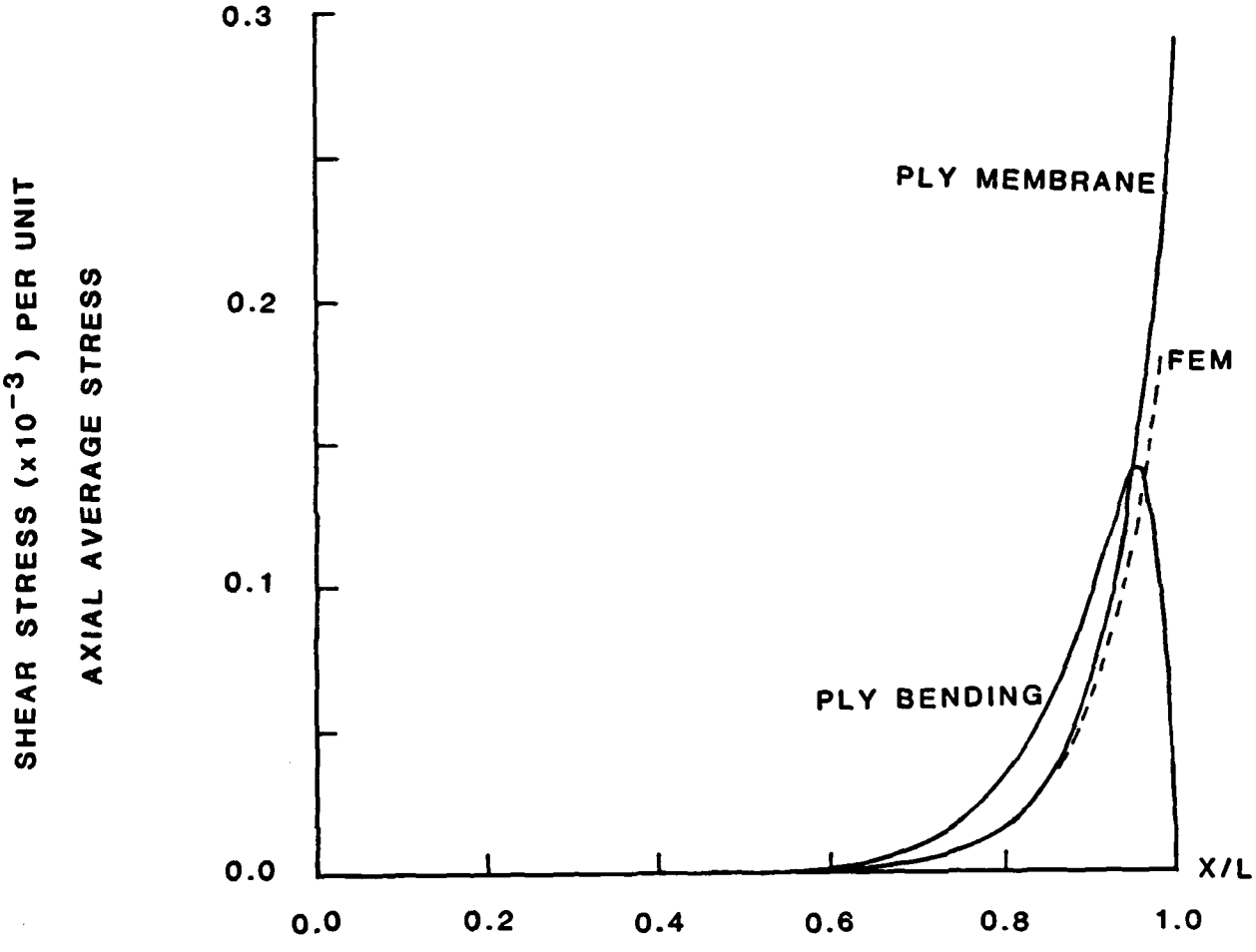
SHEAR STRESS (x10^{-3}) PER UNIT AXIAL AVERAGE STRESS
0.3
0.2
0.1
0.0
0.0
0.2
0.4
0.6
0.8
1.0
X/L
PLY MEMBRANE
FEM
PLY BENDING

FIG. 4a

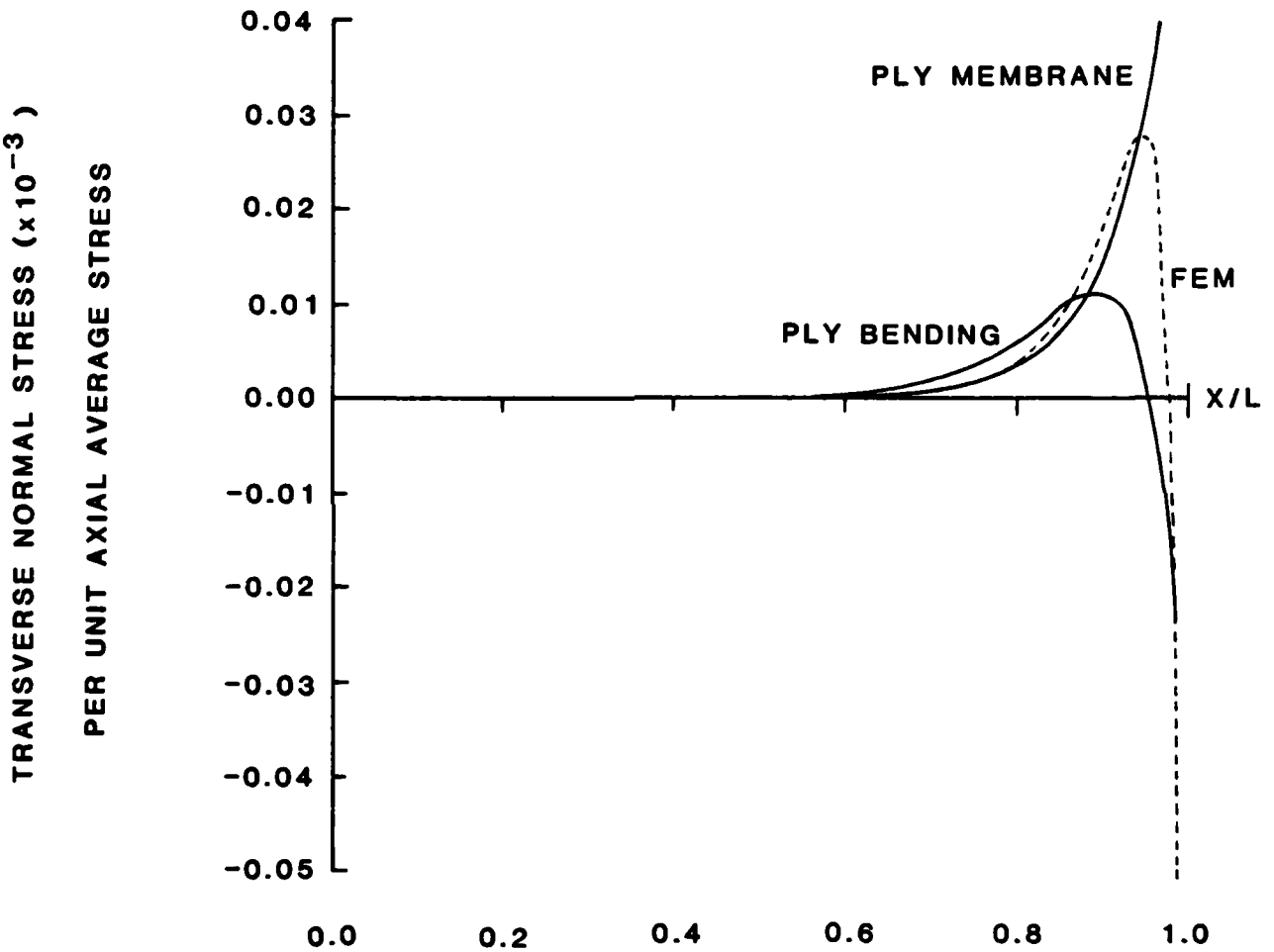
TRANSVERSE NORMAL STRESS (x10^{-3})
PER UNIT AXIAL AVERAGE STRESS
0.04
0.03
0.02
0.01
0.00
-0.01
-0.02
-0.03
-0.04
-0.05
0.0
0.2
0.4
0.6
0.8
1.0
PLY MEMBRANE
FEM
PLY BENDING
X/L

FIG. 4b

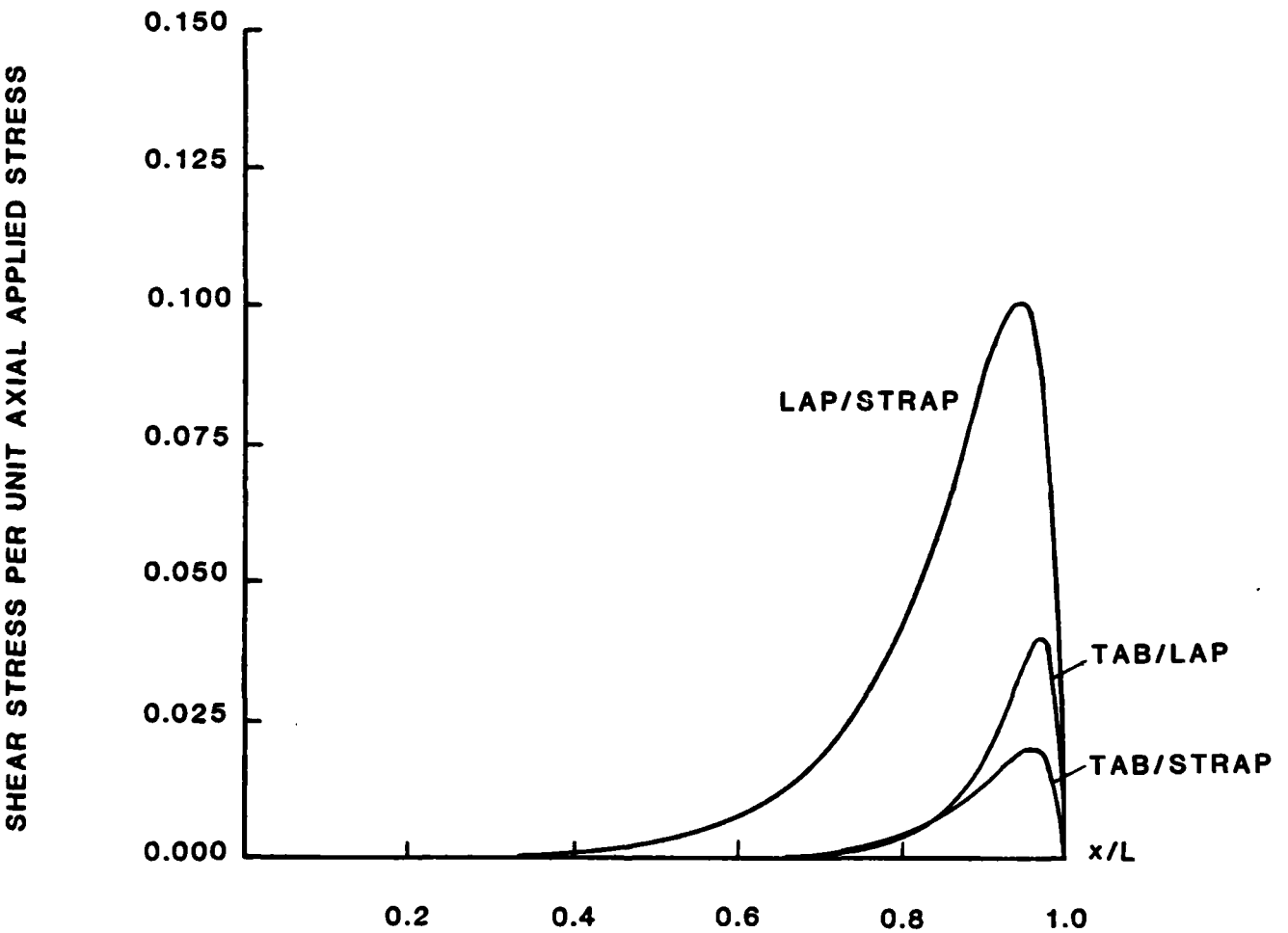
SHEAR STRESS PER UNIT AXIAL APPLIED STRESS
0.150
0.125
0.100
0.075
0.050
0.025
0.000
LAP/STRAP
TAB/LAP
TAB/STRAP
x/L
0.2
0.4
0.6
0.8
1.0

FIG. 5

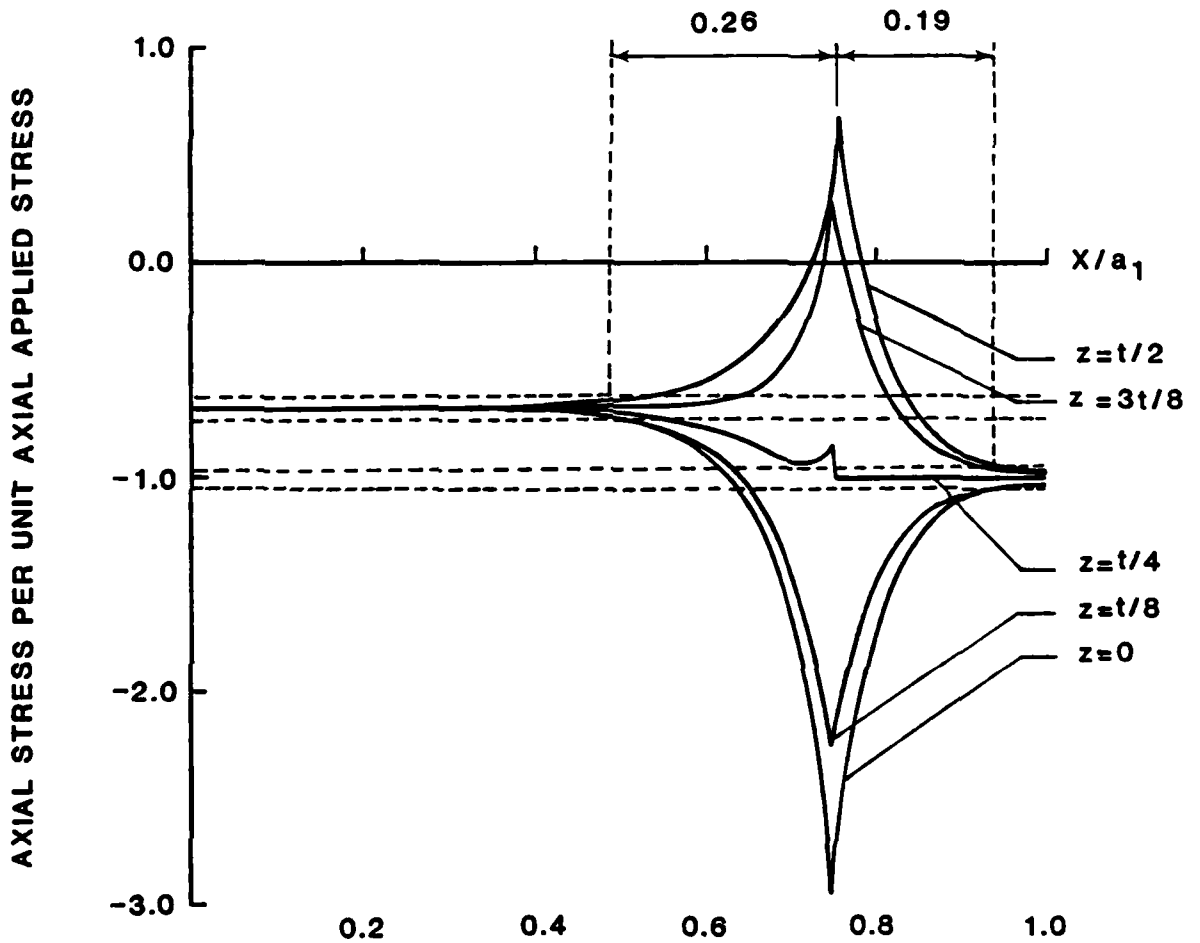
0.26
0.19
1.0
0.0
-1.0
-2.0
-3.0
X/a1
z=t/2
z =3t/8
z=t/4
z=t/8
z=0
0.2
0.4
0.6
0.8
1.0
AXIAL STRESS PER UNIT AXIAL APPLIED STRESS

FIG. 6

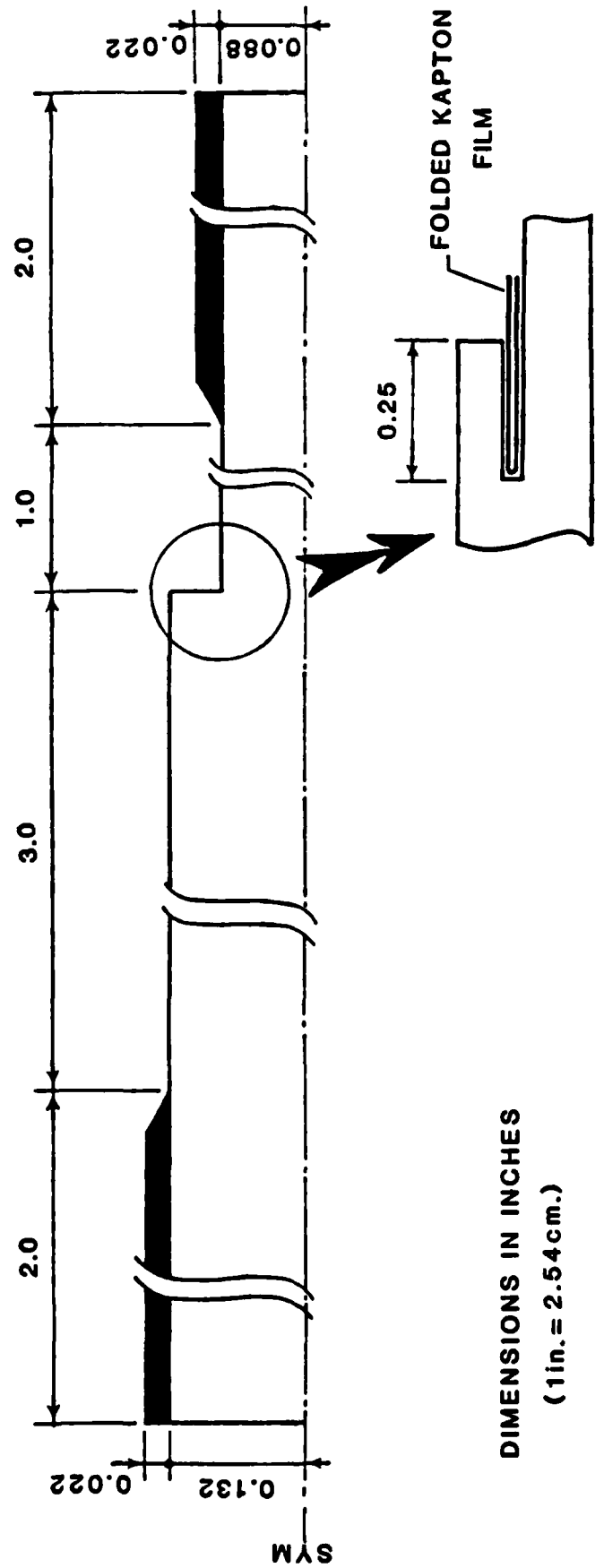
0.088
0.022
2.0
1.0
3.0
2.0
0.25
FOLDED KAPTON FILM
0.022
0.132
SYM
DIMENSIONS IN INCHES
(1in.= 2.54cm.)

FIG. 7

FIG. 10

FIG. 9

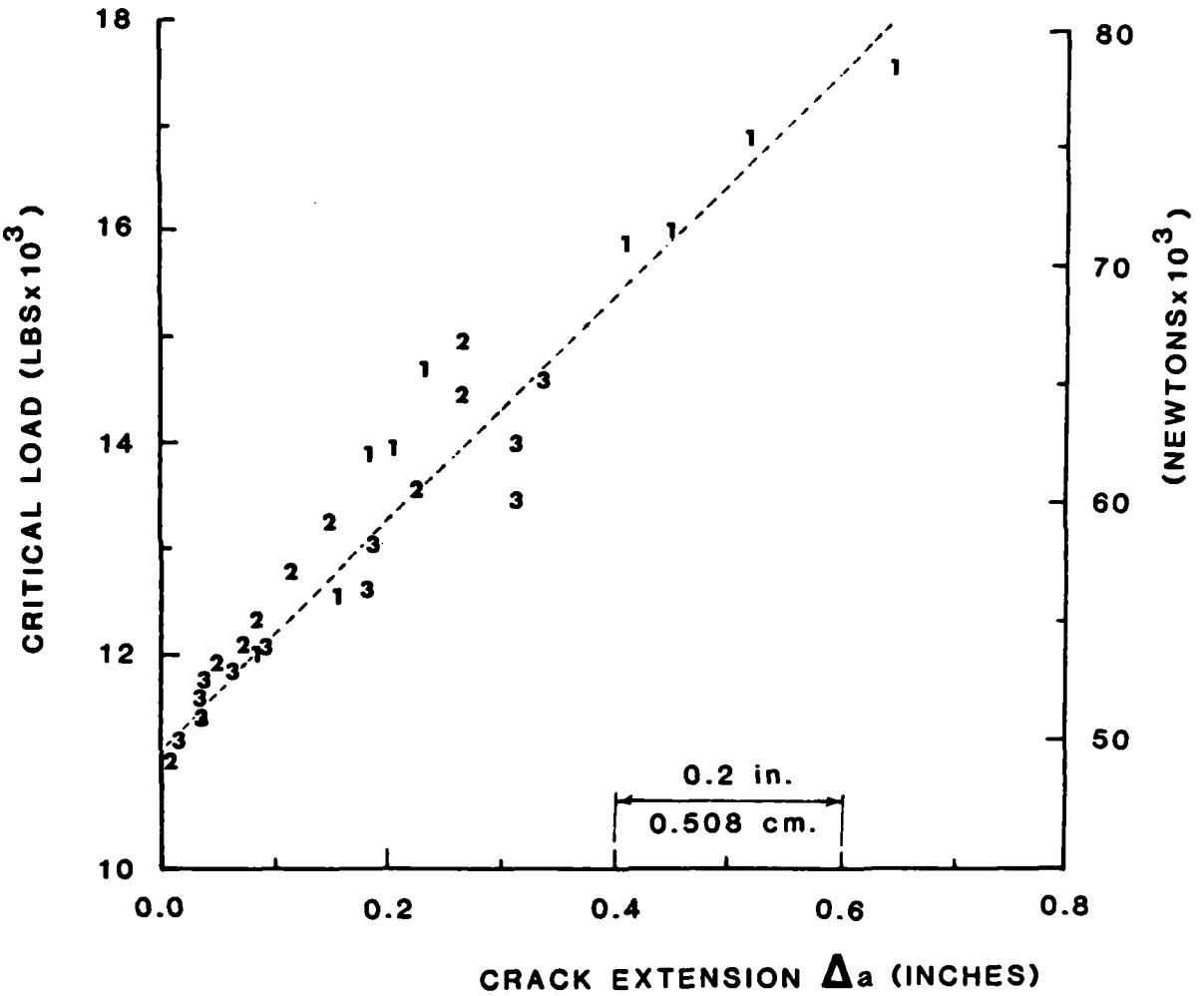
CRITICAL LOAD (LBSx10^3)
(NEWTONSx10^3)
CRACK EXTENSION Δa (INCHES)
0.2 in.
0.508 cm.
18
16
14
12
10
80
70
60
50
0.0
0.2
0.4
0.6
0.8

FIG. 11

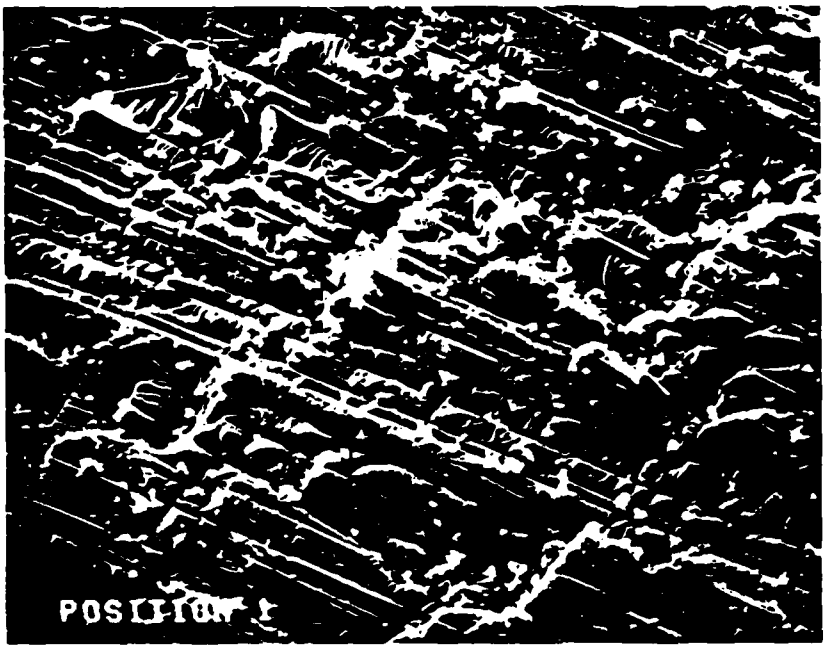

FIG. 12a

FIG. 12b

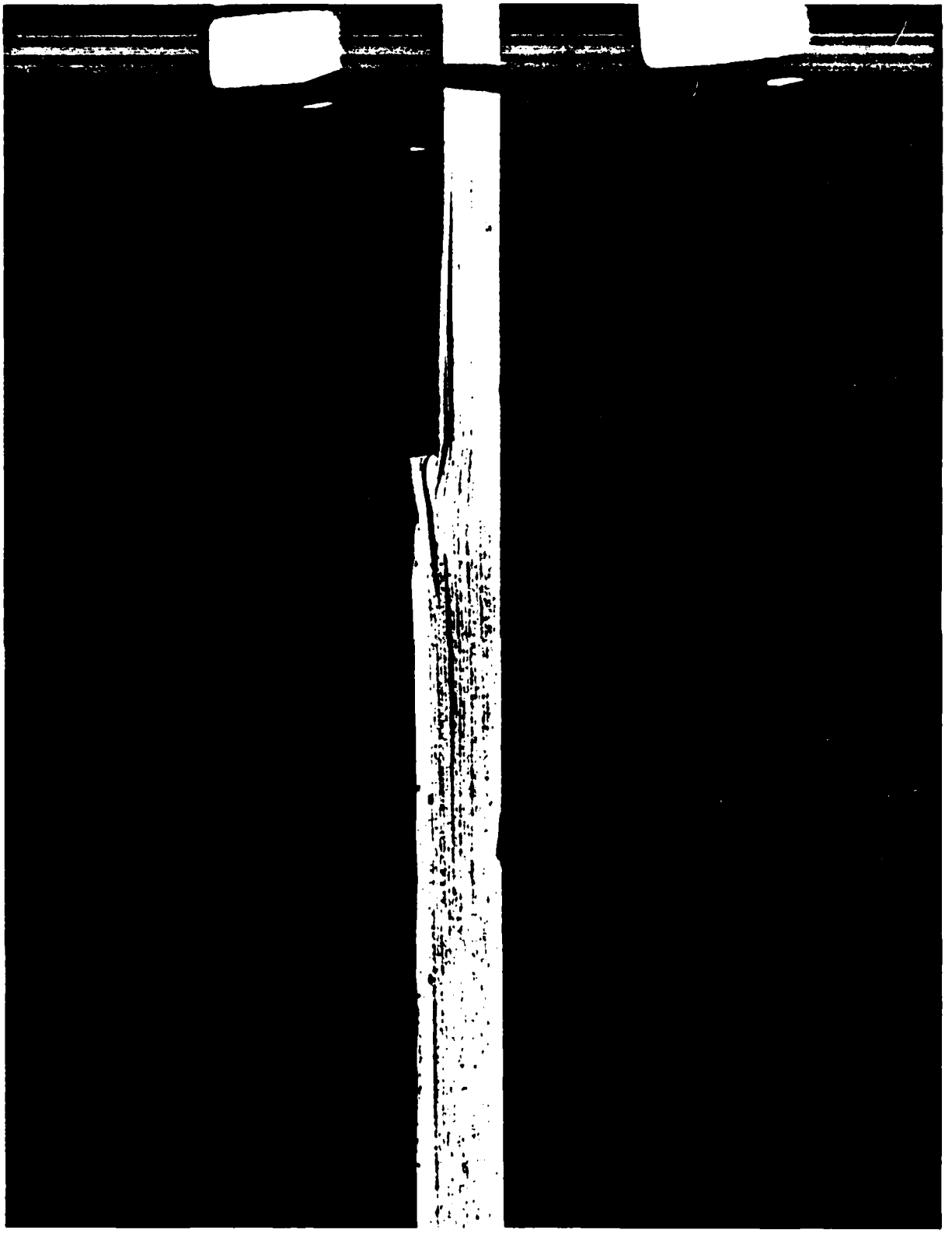

FIG. 13

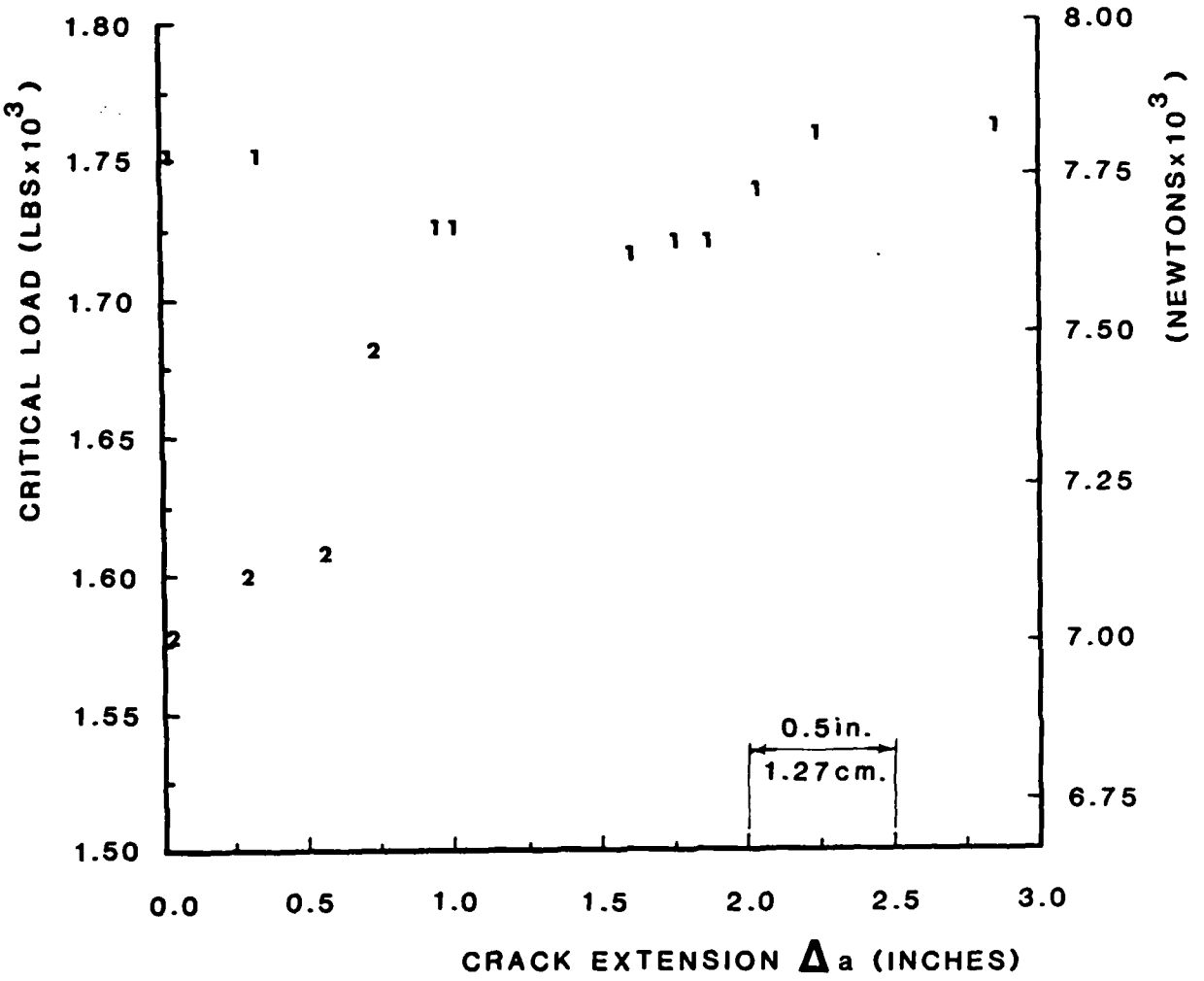
1.80
1.75
1.70
1.65
1.60
1.55
1.50
CRITICAL LOAD (LBS x 10^3)
8.00
7.75
7.50
7.25
7.00
6.75
(NEWTONS x 10^3)
0.5in.
1.27cm.
0.0
0.5
1.0
1.5
2.0
2.5
3.0
CRACK EXTENSION Δa (INCHES)

FIG. 14

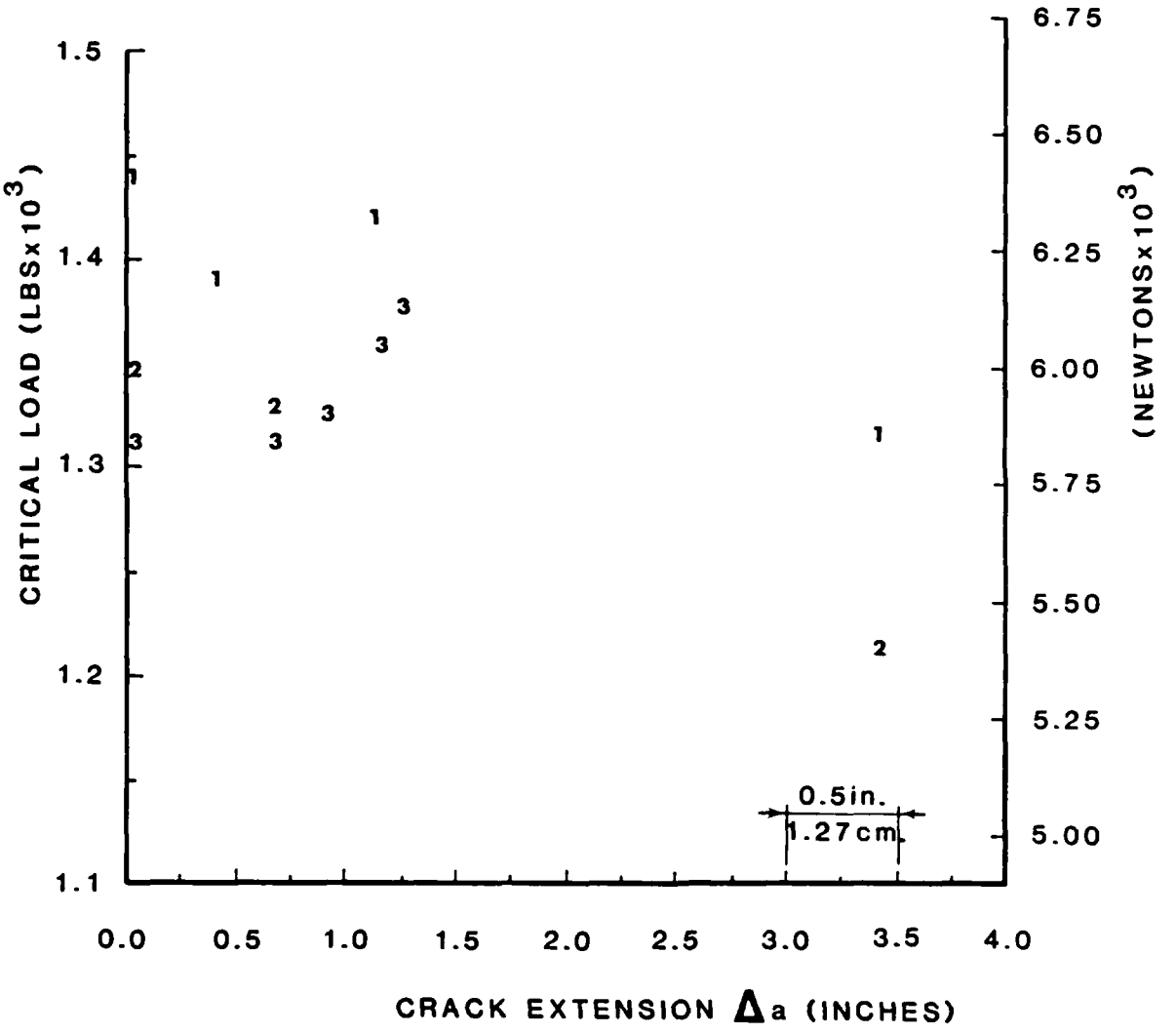
CRITICAL LOAD (LBSx10^3)
(NEWTONSx10^3)
CRACK EXTENSION Δa (INCHES)
1.5
1.4
1.3
1.2
1.1
6.75
6.50
6.25
6.00
5.75
5.50
5.25
5.00
0.0
0.5
1.0
1.5
2.0
2.5
3.0
3.5
4.0
0.5in.
1.27cm.

FIG. 15

END

FILMED

3-85

DTIC